AD-A236 059

WHOI-91-06

(2)

Woods Hole Oceanographic Institution

Ocean Response to a Hurricane, Part II: Data Tabulations and Numerical Modeling

by

James F. Price, Thomas B. Sanford and George Z. Forristall

DTIC
ELECTE
MAY 29 1991
S B D

January 1991

Technical Report

Funding was provided by the Office of Naval Research under grant No. N00014-89-J-1053.

Approved for public release; distribution unlimited.

91-00635

91 5 28 068

WHOI-91-06

Ocean Response to a Hurricane, Part II: Data Tabulations and Numerical Modeling

by

James F. Price
Woods Hole Oceanographic Institution
Woods Hole, Massachusetts 02543

Thomas B. Sanford
Applied Physics Laboratory and School of Oceanography
University of Washington
Seattle, Washington 98105

and

George Z. Forristall
Shell Development Company
Houston, Texas 77001

January 1991

Technical Report

Funding was provided by the Office of Naval Research
under grant No. N00014-89-J-1053.

Reproduction in whole or in part is permitted for any purpose of the
United States Government. This report should be cited as:
Woods Hole Oceanog. Inst. Tech. Rept., WHOI-91-06.

Approved for publication; distribution unlimited.

Approved for Distribution:

James Luyten, Chairman
Department of Physical Oceanography

Extended Abstract

Field observations of the ocean's forced stage response to three hurricanes, Norbert (1984), Josephine (1984) and Gloria (1985), are analyzed and presented in a storm-centered coordinate system. The data are simulated with two different numerical ocean models.

All three hurricanes had a non-dimensional speed of O(1) and produced a strongly rightward biased response of the ocean surface mixed layer (SML) transport and current. This asymmetry arises because the wind stress vector rotates clockwise on the right side of the track and remains nearly parallel with the inertially rotating SML current during most of the hurricane passage. The maximum layer-averaged SML currents varied from 0.8 m s^{-1} in response to Josephine, which was a fairly weak hurricane, to 1.7 m s^{-1} in response to Gloria, which was much stronger. In these two cases the current amplitude is set primarily by the strength of the wind stress and its efficiency of coupling with the SML current, and the depth of vertical mixing of the SML — all of which are local phenomena that can be accounted for in a one-dimensional model. However, in the Norbert case where the SML Burger number was appreciable, $\simeq 1/2$, the SML current was also affected by significant pressure-coupling with the thermocline — an inherently non-local phenomenon. The observations and the results from a three-dimensional simulation model show appreciable upwelling by inertial pumping and strong thermocline-depth currents, up to 0.3 m s^{-1}, under the trailing edge of Norbert.

The observed SML current has a vertical shear in the direction of the local wind of about 0.01 s^{-1} beneath the high stress regions of the hurricanes. This vertical shear causes the surface current to be larger than the layer-averaged SML current described above by typically 0.2 m s^{-1}, and has been simulated with some success by a one-dimensional turbulence closure model.

Contents

Extended Abstract i

List of Tables iv

List of Figures iv

1 Introduction 1

2 The Hurricanes 3

2.1 Surface Stress Estimation for Norbert and Josephine 4

2.1.1 Flight Level and Surface Winds 4

2.1.2 Fitting and Translation of Model Hurricanes 4

2.1.3 Calculation of Surface Stress 8

2.1.4 Norbert and Josephine Hurricane Tracks 8

2.2 Surface Stress Estimation for Gloria 8

2.3 Comments on the Wind Stress 11

2.4 Comparison of the Hurricanes 13

3 The Ocean Initial Condition 15

4 Numerical Models 19

4.1 Three-Dimensional Layered Model 20

4.2 One-Dimensional Model 22

5 Horizontal Structure of the Surface Mixed-Layer Response 24

5.1 Wind-Driven Transport 24

5.1.1 Rightward Bias 25

5.1.2 A Test of the Estimated Wind Stress 28

5.2 SML Current 31

5.3 Upper Ocean Mixing 34

5.3.1 SML Depth 34

5.3.2 SML Cooling 36

5.3.3 Bulk Richardson Number 37

6 Thermocline Currents **38**

7 Vertical Shear Within the Surface Mixed-Layer **44**

8 Summary and Remarks **49**

Acknowledgments **51**

References **52**

Appendix **55**

DTIC
COPY
INSPECTED
6

Accession For
NTIS GRA&I ☑
DTIC TAB ☐
Unannounced ☐
Justification
By
Distribution/
Availability Codes
Dist | Avail and/or Special
A-1

List of Tables

I Wind analysis and model fitting 5

II Position and speed of hurricane in study area 10

III Hurricane parameters 14

IV Initial temperature profiles 18

V Comparison of observed and simulated velocity and transport 29

1A AXCP station data 57

2A Three-layer model fit to Gloria profiles 61

3A AXCP data in storm-centered coordinate system 63

List of Figures

1 Hurricane tracks 9

2 Winds stress plan views and profiles 12

3 AXCP positions 17

4 Observed and simulated SML transports 26

5 Observed and simulated SML currents 32

6 SML depth, cooling and bulk Richardson number 35

7 Upwelling and thermocline-depth currents 40

8 Current and temperature profiles from Norbert AXCPs 42

9 Profile of current speed from Norbert AXCP 27 45

10 Vertical shear of SML current in the wind direction 47

11 Vertical shear as a function of wind speed 48

1A Flight track and AXCP positions for Gloria 56

2A Three-layer model fitting 58

1 Introduction

The ocean's baroclinic response to a moving hurricane can be thought to occur in two largely distinct stages — a forced stage response during the actual storm passage and a relaxation stage response during the following several weeks. These are characterized by quite different physical processes.

The forced stage response is a mainly local (depth and time dependent), non-adiabatic response of the upper ocean to intense wind stress. The ocean's response includes very large surface waves and currents, and substantial cooling of the surface mixed layer (SML) due mainly to vertical mixing (Price, 1981). The SML cooling can be observed by a variety of means, including satellite infrared imagery, and is now a well-documented phenomenon (Black, 1983; Stramma et al., 1986).

The relaxation stage response is an inherently non-local (three-dimensional and time dependent), adiabatic energy dispersion by near-inertial frequency internal waves that form a spreading wake behind a moving hurricane (Geisler, 1970; Price, 1983). Energy of the SML currents is dispersed vertically into the thermocline, and laterally away from the storm track. These inertial waves are readily observed only by direct current observations, and thus only a few case studies are now available (Brooks, 1983; Shay and Elsberry, 1987; Brink, 1989; Shay et al., 1989).

The connection between the forced stage and the relaxation stage response can be found in the horizontal structure of the forced stage wind-driven currents in the SML. In this paper we continue an analysis of the forced stage response to three open ocean hurricanes begun by Sanford et al. (1987) (hereafter, Part I). Part I described two field studies carried out in fall 1984 around hurricane Norbert in the eastern North Pacific Ocean and Josephine in the Sargasso Sea. In this follow-on report we are able to include a third data set acquired from a very similar field study carried out in fall 1985 with

hurricane Gloria, also in the Sargasso Sea. The data collection and analysis methods applied in the Gloria data were identical to those described in Part I (a brief review of analysis methods and a tabulation of Gloria data are in the Appendix). These three data sets are unique in showing the horizontal and vertical structure of the forced stage response, while also providing the means to estimate the two-dimensional and time-dependent field of surface wind stress that are required for simulations. Our scientific goals are to use these data to:

> i) describe and interpret the structure of the forced stage response, and consider how SML and thermocline currents will begin to evolve in the relaxation stage, and,
>
> ii) compare the field data with the results from two numerical ocean models that attempt to simulate the forced stage, baroclinic response.

The model solutions have proven to be a valuable guide to interpreting the observations. They help to reveal the large-scale pattern underlying the discrete AXCP (air-deployed expendable current profiler) observations, and they help also by showing the dynamical relationships among variables — SML current and sea surface cooling, and SML current divergence and thermocline current — that would be hard to appreciate from the data alone.

The practical goal of these studies was to observe and model the near surface currents that occur during the forced stage response. These currents are an important parameter in the design of offshore structures that could be subject to hurricane conditions. As a rule, offshore structures are designed to withstand the worst combination of storm-driven waves and currents that could be expected during a span of, typically, 100 years. It is thus necessary to extrapolate or model the design current from observed cases which are very likely to be less severe.

We begin in Section 2 with a description of the hurricane wind fields, and continue in Section 3 with the ocean initial condition, both of which are important in determining

the amplitude and structure of the response. In Section 4 we briefly introduce two numerical ocean models used to simulate the ocean response. The first model is three-dimensional and simulates the full horizontal structure of the response, but at the expense of representing vertical structure with only four layers (Price, 1981; termed '3-D'). The second model has very high resolution in the vertical dimension only, and is useful for examining the vertical shear of current within the SML (Mellor and Durbin, 1975; termed '1-D'). In Section 5 we describe the horizontal structure of the forced stage SML response, and compare observations with the 3-D model simulations. In Section 6 we consider the coupling between the SML and the thermocline that makes up the relaxation stage response. The vertical structure of the SML current and density are analyzed in Section 7 along with 1-D model simulations. In the final section, 8, we summarize results and suggest where future research might be useful.

2 The Hurricanes

The NOAA P3 aircraft that carried out the AXCP surveys described in Part I also made measurements of the flight level wind speed, wind direction, and pressure. Flight level varied considerably between the three cases; flight level was 1500 m in Norbert, 500 m in Josephine, and considerably higher in Gloria, 3300 m, because of severe turbulence. Because the Norbert and Josephine data were taken within the planetary boundary layer (PBL), we can attempt to estimate surface winds from a simple extrapolation procedure which would not be appropriate in the Gloria case. In the latter case we use the results from a hindcast simulation of the hurricane PBL.

2.1 Surface Stress Estimation for Norbert and Josephine

2.1.1 Flight Level and Surface Winds

Flight level winds were sampled at very rapid intervals along each of the radial sections flown through the hurricanes. These data were subsampled to provide a wind vector at roughly 10 km intervals (Figure 11 of Part I). These subsamples were taken when the aircraft was in a more or less steady attitude to minimize measurement errors. The largest flight level winds observed in Norbert were about 115 knots when the central pressure was about 950 mb, and the largest winds in Josephine were about 85 knots when the central pressure was about 974 mb. Thus Norbert was a moderately intense hurricane, while Josephine was somewhat weaker.

To calculate surface stress we must extrapolate the flight level winds to some standard height near the surface, here taken to be 10 m. This extrapolation is done by a simple reduction of amplitude estimated from an empirical (Bates) profile given by Powell (1980), and by a rotation of the wind vector toward lower pressure estimated from Frank's (1977) data. Because flight level was somewhat higher in Norbert, the amplitude reduction and vector rotation are both slightly larger than were appropriate for Josephine, Table I. The uncertainty in the amplitude reduction was estimated from the error bars on the original figures of Powell (1980).

2.1.2 Fitting and Translation of Model Hurricanes

The 3-D model requires a two-dimensional field of wind stress at all time steps, and hence these observed winds have to be analyzed onto a regular grid. We chose to fit these data to a model hurricane (rather than interpolate onto a grid) because the front left half of Josephine was not sampled, and, also because a fitting procedure yields a much more portable result. The form of the model hurricane was taken to be

TABLE I

Wind Analysis and Hurricane Model Fitting

Extrapolation to 10 m height

	Norbert	Josephine
Nominal flight Level, m	1500	500
Amplitude Reduction, percent	33 ± 7	27 ± 7
Rotation, deg	16	10

Model Hurricane Radial Profiles

Radius normalized by R_{max}	Wind Speed normalized by U_{max}	Inflow Angle deg
0.	0.	0
0.4	0.1	2
0.7	0.5	4
0.8	0.8	6
0.95	0.95	7
1.0	1.0	7
1.35	0.97	14
2.7	0.72	23
4.05	0.54	24
5.4	0.44	22
6.75	0.4	21
8.1	0.36	21
10.8	0.27	21
13.5	0.23	21
27.0	0.	20

Best Fit Parameters

	Norbert	Josephine
Radius to maximum wind, R_{max}, km	20 ± 2	52 ± 3
Maximum wind speed, U_{max}, m s^{-1}	36 ± 2	29 ± 2
Percent variance accounted for	93	94
Rms error of the fit, m s^{-1}	6	6

the composite hurricane compiled by NOAA/NWS (1979) for use in design studies. This model hurricane is specified by wind speed and inflow angle as a discrete function of radius in Table I. The radius is normalized by the radius to maximum wind speed, R_{max}, and wind speed is normalized by the maximum wind speed, U_{max} (dimensional values given below).

Translation of a hurricane will induce an asymmetry of wind speed, with larger values occurring on the right side of the track where the cyclonic winds and the hurricane translation add constructively. To account for this, the along track component of wind in the model hurricane is increased on the right side (and decreased on the left side) by an amount $1.17\ U_h^{0.63}$ suggested by NOAA/NWS (1979) (and ignoring the dimensions on U_h for this purpose only). Because Norbert and Josephine were moving fairly slowly when surveyed, $U_h \simeq 4$ m s^{-1}, the estimated asymmetry in wind speed induced by the translation is also fairly small, only about 2.5 m s^{-1}, but does make a noticeable difference in estimated stress.

The model hurricane (including the asymmetry noted above) was fitted to the 10 m winds by varying R_{max} and U_{max} to minimize the mean square difference between the observed winds and the model hurricane winds. The best fit R_{max} and U_{max} for each hurricane are listed in Table I along with the percent variance accounted for by the best fit model, and the root mean squared (rms) wind velocity that could not be accounted for by the best fit. In both cases the percent variance accounted for was in excess of 90%, suggesting that the NOAA/NWS (1979) model hurricane was appropriate for Norbert and Josephine. Visual comparison of the observed and fitted winds gives the same impression. There are, of course, mesoscale variations of the observed wind which are not included in the model hurricane. However, these are small compared to the largest winds, and do not have a systematic, hurricane-scale pattern.

2.1.3 Calculation of Surface Stress

The surface stress, $\boldsymbol{\tau}$, was calculated from the model 10 m wind, $\boldsymbol{U}_{10}$, using the usual bulk transfer formula, $\boldsymbol{\tau} = \rho_a C_d U_{10} \boldsymbol{U}_{10}$, where ρ_a is the density of air, and the drag coefficient C_d is the Large and Pond (1981) neutral form; $C_d = 1.14 \times 10^{-3}$ if $U_{10} < 10$ m s^{-1}, and, $C_d = (0.49 + 0.065U_{10}) \times 10^{-3}$ if $U_{10} > 10$ m s^{-1}. This form is very similar to that inferred from hurricane wind observations using the ageostrophic method by Miller (1964) (and see also Powell, 1980). In these cases the wind speed dependence of C_d is important inasmuch as the calculated C_d at the largest wind speeds, 35 m s^{-1}, is about 2.7×10^{-3}, or roughly twice the usual low wind speed value.

2.1.4 Norbert and Josephine Hurricane Tracks

Both Norbert and Josephine moved along rather complicated tracks as they passed over the study regions. Model experiments have shown that course or translation speed changes are important if they cause a change in stress direction (as seen from the ocean) of more than about 20 deg, or equivalently, if they cause a change in hurricane residence time of more than about one hour. In these cases then, it was necessary to translate the model hurricanes over the observed tracks, which were obtained from satellite and aircraft reconnaissance by the NOAA P3 (Figure 1). The 3-D model integration was begun when the hurricanes were well outside the survey region, and continued until the hurricanes reached the central positions of the surveys given in Table II. At that point the integrations were stopped, and the solutions saved.

2.2 Surface Stress Estimation for Gloria

Because the flight level in Gloria was at 3300 m and above the planetary boundary layer, we have not applied the simple extrapolation and model fitting procedure

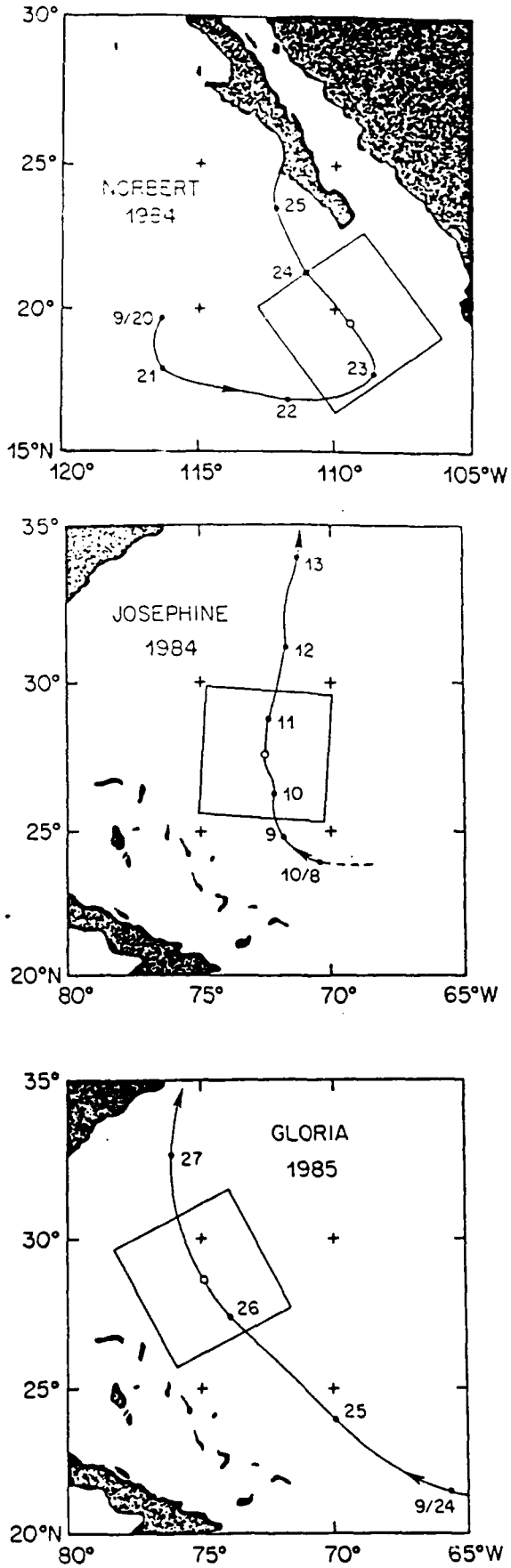

Figure 1. Tracks and survey regions (shaded) of Norbert, Josephine, and Gloria. Date is shown at 0000 UTC at daily intervals along the track.

TABLE II

Position and Speed of Hurricane in Study Region

	Norbert	Josephine	Gloria
Time and date, UTC	0112, 24 Sep.	0941, 11 Oct.	0700, 26 Sep.
Position	19.41N, 109.08W	29.41N, 72.13W	28.75N, 74.98W
Translation speed, U_h, m s^{-1}	4.1 ± 0.3	3.5 ± 0.2	6.8 ± 1.0
Course, deg T	320 ± 5	10 ± 5	333 ± 5

described above. Instead, the Gloria stress field was estimated for this project by Dr. V. J. Cardone of Oceanweather Inc. using a numerical model of the planetary boundary layer below a translating, atmospheric vortex. The time-dependent pressure field of the vortex and the synoptic scale environment were specified from observations at 30 min intervals. The model then computed the winds and the surface stress by means of a similarity theory of the marine boundary layer, and provided the field of surface stress on a regular, fixed grid.

A series of validation tests (Cardone and Ross, 1979; Cardone et al., 1980; Forristall et al., 1977; Forristall et al., 1978) indicate that this method produces hourly average surface winds that are generally accurate to within about 2 m s^{-1} in magnitude, and 20 degrees in direction. This is comparable to the uncertainty inherent in the extrapolation procedure described above.

We have also had the Norbert and Josephine pressure data sets run through the Oceanweather analysis, and found that the stress fields were very similar to those estimated from the extrapolation procedure. Comparisons showed that the maximum stress occurred at slightly larger radius (by about 10 to 15%), but that the maximum stress value was almost identical, as was the overall storm size. The end result was that the ocean models gave virtually the same simulations as when driven with the wind fields described above. On that basis, we presume that the Gloria wind stress fields are equivalent to those from the analysis of Norbert and Josephine.

2.3 Comments on the Wind Stress

In each model hurricane the largest stress occurs in the right front quadrant because of the asymmetry induced by translation (Figure 2, right panels). The left to right asymmetry of stress is about 35%, which is enough to make a detectable difference in the simulated currents. However, as we will see in Section 5, the rightward asymmetry

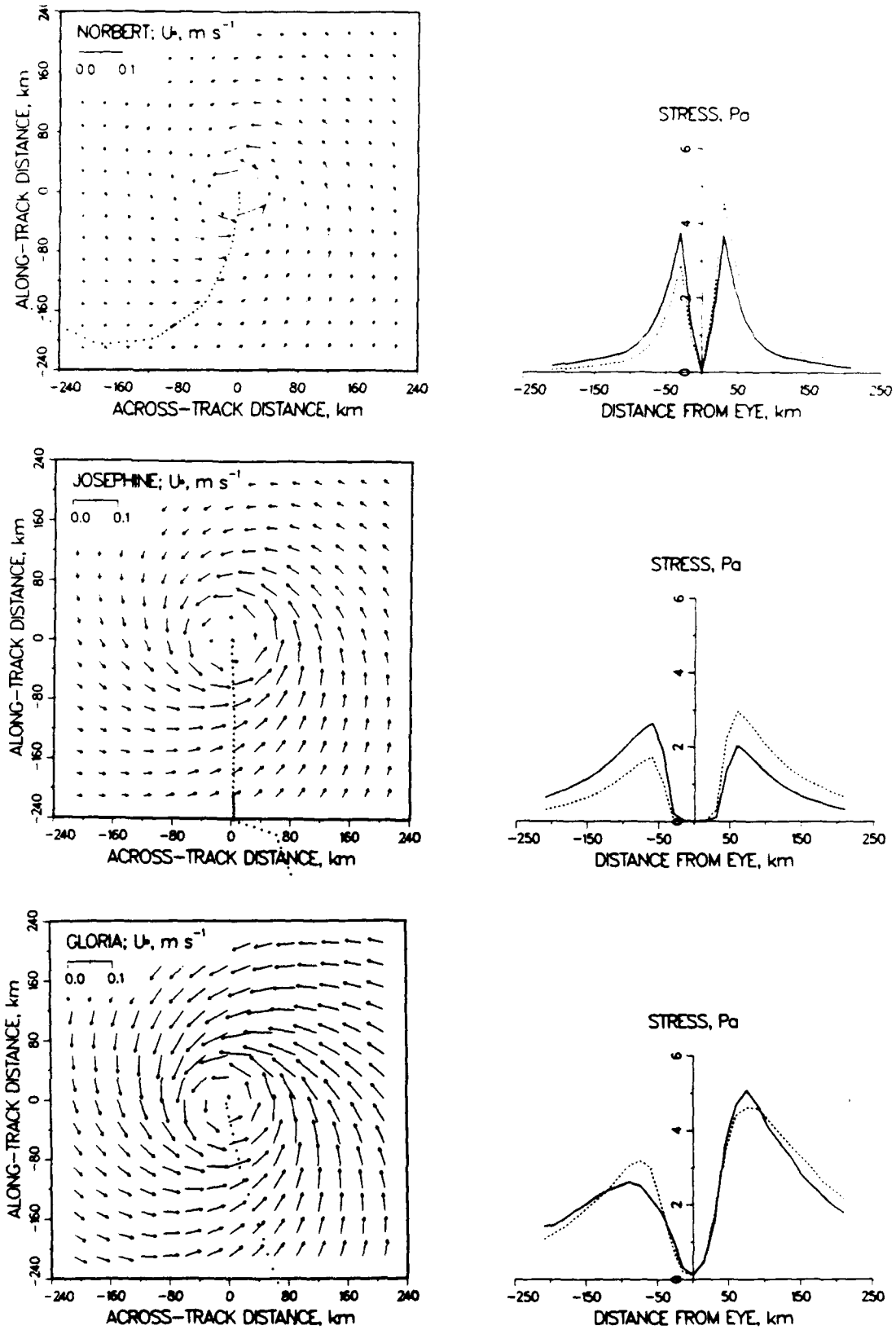

Figure 2. Wind stress for hurricanes Norbert, Josephine, and Gloria (top to bottom) shown as friction velocity in plan view (left column) and in cross section through the hurricanes (right column; solid line is a slice along the track, dashed line is across the track). In all plan view figures the hurricane is centered in the figure, and coordinates are rotated so that hurricane translation is in the positive along track direction. The dotted lines are the hurricane tracks at 2000 second intervals.

in the current response is much larger than this (roughly a factor of five) on account of an inherent asymmetry in the coupling between the surface stress and the near-inertial current in the SML.

It is important to keep in mind that the wind stress estimated by either of the methods described above is most directly related by calibration of the aerodynamic formula to the stress in the marine planetary boundary layer (PBL), and not to the stress within the SML that we need to know to model currents. Moreover, the bulk formula and drag coefficient are calibrated for more or less steady conditions in which surface waves can be assumed to be a transparent intermediary in the momentum transfer from the wind to the surface current (Stewart, 1974). In hurricane conditions surface waves are presumably quite non-stationary, and could possibly lead to a non-local momentum transfer from the PBL to ocean currents. This raises the following question that we can attempt to answer with these data.

> *Question 1: Is the hurricane wind stress estimated from the bulk formula absorbed locally by ocean currents?*

This will be taken up in Section 5 when we examine the transport in the SML.

2.4 Comparison of the Hurricanes

The hurricanes can be characterized by the three parameters R_{max}, U_h, and the stress amplitude, τ, that are listed in Table III along with a scale estimate of the SML current amplitude and the upwelling amplitude (Price, 1983; Greatbatch, 1984). The primary difference between these hurricanes is in their size; Norbert was a fairly compact hurricane having $R_{max} = 20$ km, while Gloria was both large, having $R_{max} =$ 75 km, and also quite powerful.

TABLE III

Hurricane Parameters

	Norbert	Josephine	Gloria
U_h, m s^{-1}	4.1	3.5	6.8
R_{max}, km	20	52	75
τ, Pa (a)	4.0	2.5	4.0
f, s^{-1}	4.8×10^{-5}	7.1×10^{-5}	7.0×10^{-5}
h_1, m (b)	40	60	50
$\tilde{U}_1 = \frac{\tau R_{max}}{\rho_0 h_1 U_h}$, m s^{-1} (c)	0.47	0.60	0.86
$\tilde{\eta}_1 = \frac{\tau}{\rho_0 f U_h}$, m (d)	20	10	8
$S = \frac{U_h}{2f R_{max}}$	2.1	0.5	0.6
$M = \frac{g' h_1}{4f^2 R_{max}^2}(1 + \frac{1}{S^2})$ (e)	0.5	0.2	0.07
$Q = \frac{3\tau}{\rho_0 h_1 U_h f}$	1.5	0.5	0.5

Notes:

(a) An average of the maximum values on the left and right sides of the hurricane

(b) Typical values of z_1

(c) This is a scale for SML current. Even in a linear case the actual maximum current depends also upon S and M, but for $S > 1$, the maximum current is about $2\tilde{U}_1$.

(d) Scale for the amplitude of inertial pumping. Same comment holds as for $\tilde{U}$; actual maximum is about $2\tilde{\eta}_1$.

(e) The reduced gravity of the thermocline, g', is taken to be $4 \times 10^{-3} g$ in each case.

Some qualitative aspects of the ocean's response can be anticipated from the following three non-dimensional parameters formed from the characteristic scales of the hurricanes and the ocean's stratification (Table III). These are:

1) S, the non-dimensional storm speed, which is the ratio of the hurricane residence time to the local inertial period. S is O(1) in each case, so that the wind stress seen from the ocean changes on a time scale comparable to the local inertial period. As a consequence, we would expect that the SML current should be dominated by inertial motions, rather than geostrophic currents which would be more important at smaller S.

2) M, a Burger number for the SML, which is the ratio of the pressure gradient force to the Coriolis force acting upon the SML current. Given the large M in the Norbert case, we would expect that pressure-coupling between the SML and thermocline would be most pronounced in that case.

3) Q, a Rossby number for the SML current, which is the ratio of horizontal advection of momentum to the Coriolis force. Again, the small size of Norbert would be expected to lead to enhanced non-local effects during the forced stage response.

3 The Ocean Initial Condition

In order to analyze the data and run the ocean models we have to specify the ocean initial condition over the study regions. In principal this should include the fields of temperature, salinity, and current. In practice though, the aircraft and instrument resources required to obtain such data were not available, and even if they had been, it would have been problematic to forecast the hurricane track well enough to carry out a useful survey. In the absence of a complete initial survey we are forced to make the following three assumptions, the last two of which are dubious in the Josephine and Gloria cases. We assume that:

1) salinity played no important role in the density stratification,

2) the temperature profile was horizontally homogenous, and could be estimated from AXCP temperature profiles made under the leading edge of the hurricanes (Figure 3: Norbert AXCPs 2, 4, and 31; Josephine AXCPs 20, 21, 7, 3, and 4; Gloria AXCPs 31, 17 and 18), and that

3) pre-hurricane currents in the survey regions were negligible.

The estimated initial temperature profiles are listed in Table IV, along with uncertainties estimated from the variability among the AXCPs noted. This uncertainty does not include possible inhomogeneity. As noted in Part I, satellite imagery from the Sargasso Sea (NWS/NESS Oceanographic Analysis) shows significant pre-hurricane horizontal variability due probably to the subtropical front (Voorhis, 1969; and see Black et al., 1988 for direct observations relevant to the Josephine case). Evidence of this in AXCP data is coolest surface temperatures found ahead of the hurricanes (north of the front), which can not be attributed to the hurricane response, and thermocline-depth isotherm displacements and currents which are similarly incompatible (coolest temperatures and largest thermocline-depth currents ahead of the hurricane). As a result, the interpretation of the thermal field and thermocline current data from the Sargasso Sea cases (Josephine and Gloria) is problematic. For those fields we emphasize the Norbert data set which evidently had much less pre-hurricane variability.

The neglect of initial currents will introduce an error or uncertainty in our analysis about which we can say very little. We suspect that the resulting error is as large as the uncertainly associated with the AXCP measurement or analysis method (about 0.2 m s^{-1}, Part I). One can assume that SML currents of O(0.2 m s^{-1}) are likely to be found at any open ocean site, and we have to assume that such currents could be

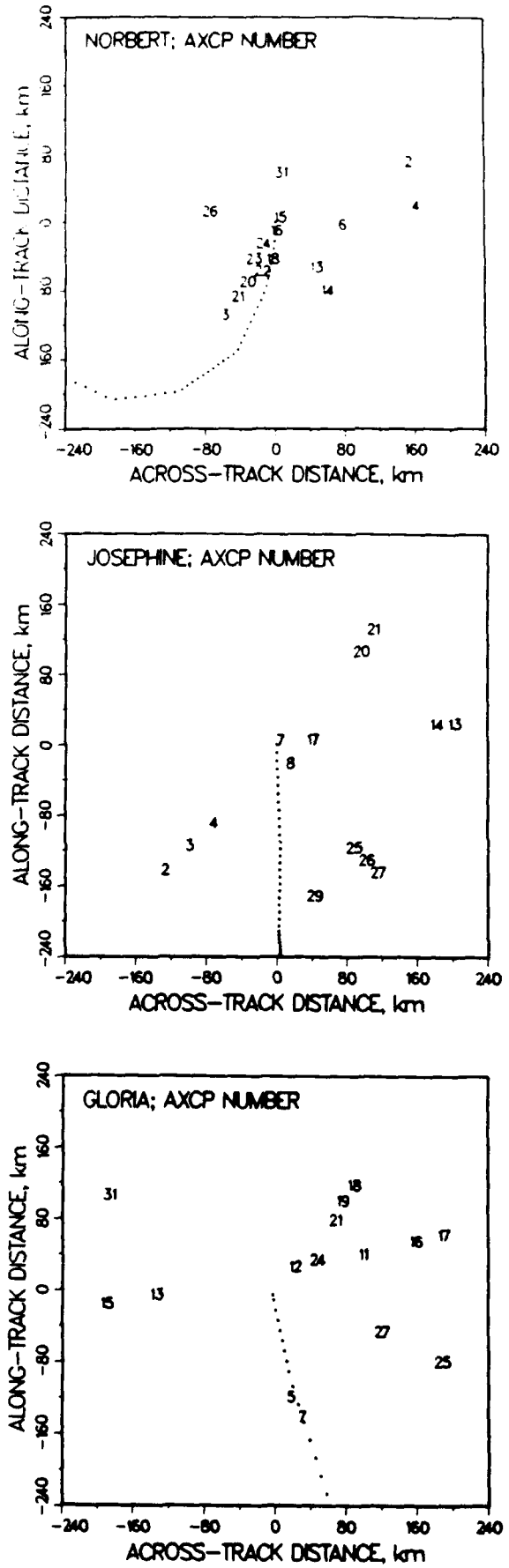

Figure 3. AXCP profile numbers.

TABLE IV

Initial Temperature Profiles

	Norbert	Josephine	Gloria
Latitude, deg.	19	29	29
Sea surface temperature, C	28.5	27.0	28.5
Mixed-layer thickness, m	25 ± 5	35 ± 10	40 ± 5
Temperature jump at SML, C	1 ± 1	1 ± 1	3 ± 1
Layer two temp. grad., C m^{-1}	0.16 ± 0.04	0.06 ± 0.02	0.06 ± 0.02
Layer two thickness, m	100	180	200
Layer three temp. grad., C m^{-1}	0.016	0.005	0.005
Layer three thickness, m	350	375	375
Layer four temp. grad., C m^{-1}	0.016	0.03	0.02
Layer four thickness, m	380	450	580

present and superimposed upon the total current measured by the AXCPs. The net uncertainty in interpreting the AXCP current data as if it were strictly a hurricane response is thus of O(0.3 m s^{-1}). The saving feature of this study is that the largest hurricane-driven SML currents are O(1 m s^{-1}), and are large enough to stand clearly above almost any other background variability. Thus the pattern of the hurricane-driven SML current is quite clear in all three of our data sets. Moreover, there is a significant difference in SML current between the three data sets that can be readily interpreted as a consequence of hurricane size or intensity.

4 Numerical Models

Two quite different kinds of numerical ocean models are used to simulate the response to the hurricanes. The first is a fully three-dimensional, primitive equation model described by Price (1981) (3-D), and the second is a one-dimensional boundary layer model described by Mellor and Durbin (1975) (1-D). These models complement one another in that the 3-D model simulates the full horizontal structure of the response, but attempts to represent vertical structure with only four layers of which the uppermost is the SML. The 1-D model ignores horizontal structure and thus non-local effects altogether, but attempts to simulate the detailed vertical structure within the SML which the first model ignores.

As we will show from the data in the following sections, the forced stage response is fundamentally a local process, but one which has considerable, interesting horizontal structure. While non-local dynamical effects are clearly present, especially in the Norbert case, the non-local effects are generally not of leading importance in the forced stage response, so that a 1-D model can produce useful simulations of SML currents as demonstrated by Martin (1982). Similarly, while there is some vertical shear within the SML, it is not so large as to complicate the interpretation of the 3-D model results.

(And continuing this, we see no evidence whatever that shear and non-local effects interact.) Hence it is quite possible and in some ways efficient to consider separately the questions of horizontal and vertical structure and dynamics.

Since both of these models have been described in detail before, the present discussion is limited to a consideration of which processes can be regarded as well resolved and reliable, and which model assumptions and parameterizations can and should be tested with the available data.

4.1 Three-Dimensional Layered Model

Physical assumptions and simplifications made in the Price (1981) model are as follows:

1) Density is represented by a linear state equation, and variation of density is ignored except in the hydrostatic pressure equation (Boussinesq approximation). Though the model can readily (and generally should) include salinity in the density equation, in this case no salinity data were available, and salinity is ignored. None of these assumptions is thought to be serious.

2) The Coriolis parameter f is assumed constant, as is the density stratification within the thermocline. These are acceptable for short times after the hurricane passage (less than a few days), or before the inertial wave wake has had time to disperse vertically and horizontally away from the track (Geisler, 1970; Price, 1983; Gill, 1984).

3) The sea surface is taken to be a rigid lid to exclude fast barotropic waves, and the abyssal ocean is taken to be infinitely deep (reduced gravity approximation). These approximations are appropriate for the deep, open ocean study sites considered here where the barotropic current response is expected to be very small, O(0.02 m s^{-1})

(Geisler, 1970; Cooper and Thompson, 1989a, 1989b), compared to the wind-driven current in the SML which is O(1 m s^{-1}).

4) As we have noted already, vertical structure in this model is represented by only four discrete layers (Price, 1981, Figure 4). The SML and the transition layer are represented by the top-most layer, which is in direct contact with the hurricane. The thermocline is represented by the lower three layers. Coupling between the SML and the thermocline occurs only by means of the hydrostatic, baroclinic pressure gradient produced by inertial pumping, which is a well resolved process in the model.

> *Question 2: Can the forced stage response and the early relaxation stage response be simulated by a model having only a few discrete layers?*

This is taken up in Section 6 when we examine the vertical structure of the thermocline response.

5) Finally, the only subgridscale (unresolved) process treated in the model is upper ocean vertical mixing, which in a layered model is represented by SML entrainment. Entrainment is a crucial process in the forced stage response, causing significant changes in SML thickness, and is the main process causing sea surface cooling (Price, 1981; Martin, 1982; Cornillon et al., 1987). In this model the entrainment velocity, W_e, is parameterized by the function,

$$W_e = 5 \times 10^{-4} \delta V \, R_v{}^{-4} \ , \quad \text{where} \tag{1}$$

$$R_v = \frac{g \, \delta\rho \, h_1}{\rho_0 \, \delta V^2} \tag{2}$$

is the bulk Richardson number, g is the acceleration of gravity, $\delta\rho$ is the density jump across the base of the SML, ρ_0 is a reference density, and $\delta V = V_1 - V_2$ is the change

of current across the base of the SML (layer 2 is the upper thermocline layer in the 3-D model). This form gives significant entrainment rates only when R_v is less than 1, which in practice occurs when the SML current, V_1, is strongly accelerated by the wind stress.

> *Question 9: Is the SML bulk Richardson number less than 1 in regions of strong entrainment?*

We will take this up in Section 5.3 when we examine SML cooling and the Richardson number estimated from the AXCP data.

The 3-D model was implemented on a grid with horizontal resolution of 15 km, and integrated with a time step of 900 sec, both of which are sufficient to yield a converged solution. There is no explicit diffusivity in the model, and numerical diffusivity is negligible for the short duration of these simulations.

4.2 One-Dimensional Model

The 1-D boundary layer model used here was developed by Mellor and Durbin (1975) to simulate the wind-forced evolution of upper ocean current and temperature profiles.

Physical assumptions and simplifications are as follows.

1) Turbulent fluxes of momentum and heat within the SML and transition layer are parameterized by an eddy viscosity and an eddy diffusivity. Hence, this model can simulate vertical shear within the SML. In this particular version of the model, these exchange coefficients are calculated from relatively simple algebraic equations, making this a Level 2 scheme in the terminology of Mellor and Yamada (1982). The simplifications in a Level 2 scheme include the neglect of turbulent vertical advection

and diffusion of turbulent energy. These terms should be relatively small in a wind driven boundary layer in which the turbulence production is dominated by shear.

2) The model is one dimensional, and thus ignores all of the non-local dynamics that make up the relaxation stage response — inertial pumping, horizontal pressure gradients, and horizontal advection. In the extreme cases where these effects can be fairly large (small intense hurricanes, such as Norbert), this model alone might not yield accurate simulations of the SML current. However, these non-local effects generally have a large vertical scale and contribute a nearly depth-independent current perturbation to the directly wind-driven SML current. Hence, it is plausible to treat separately the non-local effects and the issue of vertical shear within the SML.

The eddy coefficients are the product of the turbulent kinetic energy, a length scale calculated from the first vertical moment of the turbulent energy, and a stability function dependent upon the gradient Richardson number. The strong dependence upon a gradient Richardson number causes this model to have a mixing response to wind-forcing that is in some respects very similar to that of the 3-D model in which the mixing depends upon a bulk Richardson number. That is, this model also gives strong vertical mixing in circumstances where the wind stress accelerates the upper layer current to large values and thereby produces low gradient Richardson numbers over a thick, upper ocean layer.

Given the eddy viscosity and diffusivity as a function of depth, the one-dimensional equations for turbulent transport can then be solved numerically. In turn, the eddy coefficients can be calculated from the algebraic equations. The system is formally closed, but iteration is required in order to find eddy coefficients which are consistent with the mean flow. The high wind stress imposed by the hurricanes caused stability problems in the iterative solution until two smoothing operations were introduced. First the updated eddy parameters were smoothed with a three point operator, and

then the average of the new and old values of the eddy parameters was used in the bulk flow computations. Usually, fewer than ten iterations were required for convergence. In these simulations we used a vertical grid size of 4 m and a time step of 1800 sec.

The Mellor and Durbin (1975) model has been applied extensively, and verified against several upper ocean data sets, including current meter measurements in Hurricane Eloise (Martin, 1982). Our AXCP observations are particularly appropriate for testing this model since they give detailed vertical profiles of current and temperature. A specific question that we address here is

> *Question 4: Does the 1-D model give realistic solutions for vertical shear of current within the SML and transition layer?*

This will be taken up in Section 7.

5 Horizontal Structure of the Surface Mixed-Layer Response

In this section we describe the horizontal structure of the response within the SML, and compare the 3-D model solutions to the observations. We begin with a discussion of the wind-driven transport in the SML because it has simpler dynamics than does the SML current, and because the observed transport can be used to make a fairly sensitive test of the estimated wind stress.

5.1 Wind-Driven Transport

The wind-driven (volume) transport evaluated from the three-layer model fit to AXCP observations is estimated to be $\boldsymbol{D} = \boldsymbol{V}_1 h_1 + \boldsymbol{V}_2 h_2$ since layer 2 is the transition

layer over which the SML current matches to the pressure-driven current in the thermocline. The current in layer 2 is nearly always found to be parallel to the SML current, and thus the wind-driven transport is very nearly parallel to the SML current. The transport evaluated from the 3-D model solution is just $\boldsymbol{D} = \boldsymbol{V}_1 h_1$, where subscript 1 denotes the SML.

The transport vectors estimated from ACXP data are plotted in Figure 4 (left) in a storm-centered, quasi-synoptic coordinate system in which the hurricane is translating directly up the page (details are given in the last section of the Appendix). Simulations from the 3-D model are plotted in exactly the same way in Figure 4 (right). To the extent that the translation is steady, then the along-track coordinate is time-like. The major advantage of this storm-centered coordinate system is that it helps us to compare the three cases.

5.1.1 Rightward Bias

The dominant pattern in each case is a clockwise turning and acceleration of the transport vectors underneath the hurricanes, and a striking rightward bias in the amplitude (noted also in Part I and by Church et al., 1989). For example, at a position 75 km to the right of the center of Norbert the observed transport is about 60 $m^2\ s^{-1}$, while at the same distance to the left of the track the amplitude is only about 5 $m^2\ s^{-1}$. A comparable rightward bias occurs in the model solutions because of an inherent asymmetry in the coupling between the wind stress of a moving hurricane and the wind-driven SML transport. The transport (and the SML current) tend to rotate inertially (clockwise in this northern hemisphere case). On the right side of the track the wind stress also turns clockwise with time when viewed from the ocean. When S is O(1) as it is here and for most hurricanes, the wind stress rotation rate roughly matches the rotation rate of the transport (Chang and Anthes, 1978; Price, 1981), and

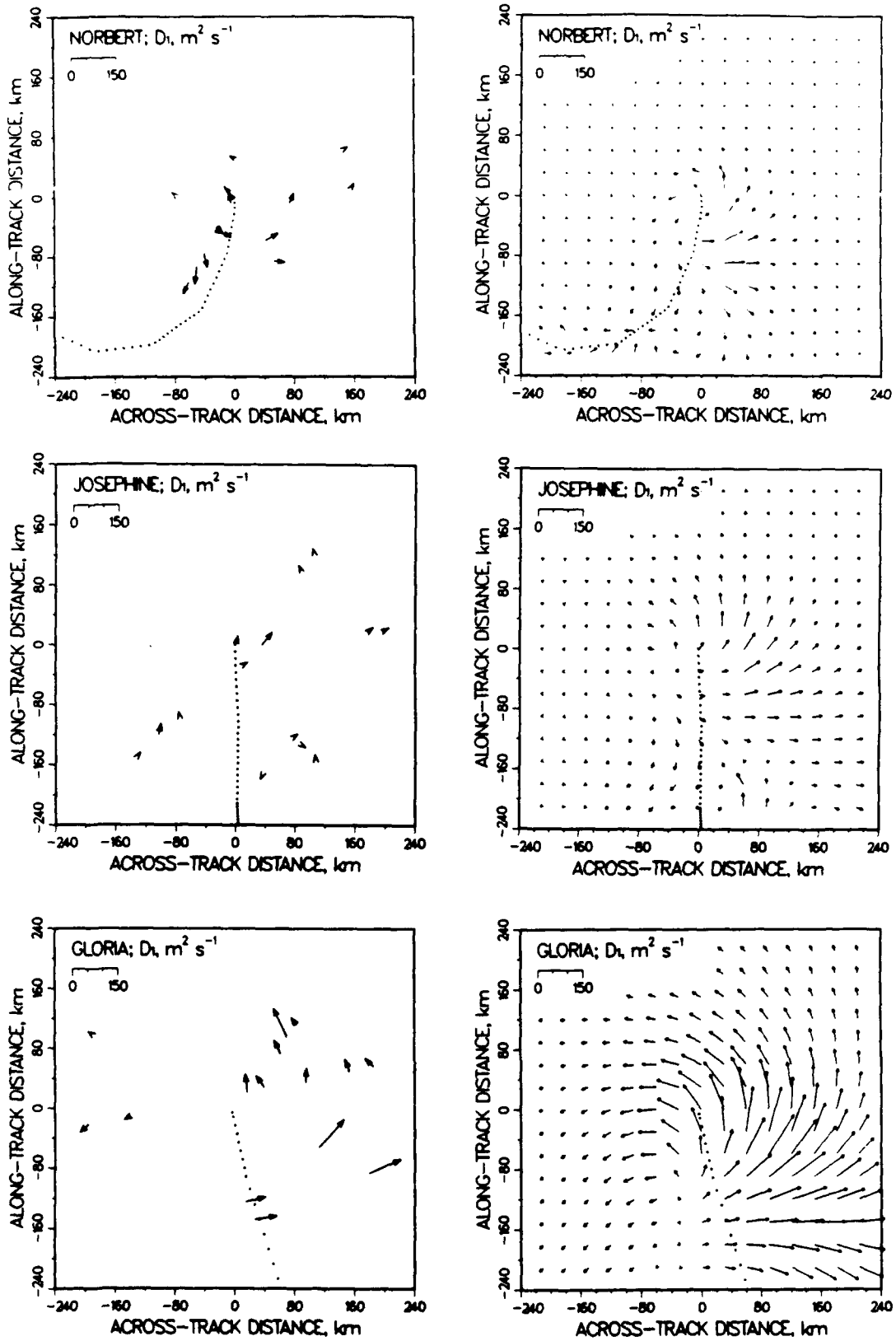

Figure 4. Transport within the SML as estimated from AXCP data (left panels), and as simulated by the 3-D model (right panels). A transparent overlay greatly facilitates the comparison of the observed and simulated fields.

the end result is that the transport and wind stress remain roughly aligned throughout most of the hurricane passage. Thus the transport is accelerated to almost the largest possible amplitude on the right side of the track.

On the left side of the track the coupling between the SML transport and the wind stress is much less efficient because the wind stress rotates anti-clockwise during the hurricane passage. Under the leading edge of the hurricane the wind stress begins to accelerate the resting ocean, but within about four hours the inertial rotation of the transport and the anti-clockwise rotation of wind stress cause the current and wind stress to be roughly anti-parallel during most of the hurricane passage. The result is that transport never becomes very large on the left side of the track.

This left-to-right asymmetry in transport amplitude is enhanced by the stronger wind stress amplitude that also occurs on the right side of a moving hurricane (Section 2.3). However, the factor of five difference in transport amplitude across the hurricane track is due overwhelmingly to the asymmetric rotation of the wind stress noted above rather than the comparatively small asymmetry of wind stress magnitude.

Notice that the very simple dynamics that lead to the left-to-right asymmetry in transport involve only the local wind stress and the local current or transport. Thus the 1-D model can also simulate this asymmetry, if driven with the appropriate time-varying wind stress (noted also by Martin, 1982), and indeed the 1-D model gives a roughly comparable result for simulated SML currents and transports (more on this in Section 7).

The storm-centered coordinate system also helps to reveal the case-to-case differences in the horizontal patterns of transport, most of which can be attributed to variations in the hurricane size or track. Notice particularly that the overall width of the region of strong response is considerably bigger in the Gloria case than in the Norbert case, and not surprisingly is directly proportional to the size of the hurricanes.

The Norbert case also shows a region of strong response to the left rear which is not seen in the other cases. This is due to the cyclonically curving track that Norbert took upon entering the survey region (Figure 1).

5.1.2 A Test of the Estimated Wind Stress

For a hurricane of a given size and moving along a given track, the simulated transport is almost directly proportional to the wind stress amplitude; it is almost completely independent of model-specific physics and parameterizations, and in particular the transport amplitude does not depend upon vertical mixing (entrainment). Simulated transport is affected somewhat by the pressure-coupling between the SML and the thermocline, but as noted in the discussion of models in Section 3, this pressure coupling is a fairly well resolved process in the 3-D model. Hence, we would expect any other three-dimensional, primitive equation model driven by the same hurricanes to yield virtually the same solutions for wind-driven transport that we show here from our 3-D model. A comparison of the observed and simulated transport thus makes a fairly sensitive test of the wind stress in near isolation from model-specific assumptions regarding physics or parameterizations.

To quantify the comparison of the simulated and observed data we have computed some simple statistics on the observed and simulated transports, and on the differences between the two, Table V. For example, a measure of the average vector difference between the observed and the simulated transport is just

$$\text{rms transport difference} = \sqrt{\frac{1}{N}\sum_{i=1}^{N}(\boldsymbol{D}_{Oi} - \beta \boldsymbol{D}_i)^2},$$

where $\boldsymbol{D}_{Oi}$ is the observed transport vector at AXCP i, $\boldsymbol{D}_i$ is the simulated transport vector at the position of AXCP i found by linearly interpolating the 3-D model solution,

TABLE V

Statistical Comparison of Observed and Simulated Velocity and Transport

	Norbert	Josephine	Gloria
rms observed transport, $m^2\ s^{-1}$	37	24 (21)*	68
rms transport difference, $m^2\ s^{-1}$	17	19 (10)	37
average transport mag. difference, $m^2\ s^{-1}$	7	0 (-2)	-7
percent variance of transport	80	38 (78)	70
rms observed velocity, $m\ s^{-1}$	0.78	0.35 (0.32)	1.05
rms velocity difference, $m\ s^{-1}$	0.28	0.30 (0.16)	0.44
average speed difference, $m\ s^{-1}$	0.16	-0.07 (-0.07)	0.06
percent variance of velocity	87	27 (75)	82

* Values in parentheses are omitting AXCPs 2, 3 and 4

N is the number of AXCPs in the ensemble average, and $\beta = 1$ here. From a similar statistic computed over the observed transport separately we can compute the percent variance accounted for by the simulated transport as $100 \times (1 - (\frac{\text{rms transport difference}}{\text{rms observed transport}})^2)$. A measure of the transport difference due solely to differences in magnitude is just

$$\text{average transport mag. difference} = \frac{1}{N}\sum_{i=1}^{N}(|\ \boldsymbol{D}_{Oi}\ | - |\ \boldsymbol{D}_i\ |).$$

These statistics show that in the Norbert and Gloria cases the simulated transport can account for about 75% of the variance in the observed transport (this is true in the Josephine case only if we are allowed some selective averaging, more on this below), and that on average over all three cases the simulated transport has about the same magnitude as the observed transport. That is, there is no evidence of a substantial bias error in stress amplitude, and specifically there is no simple scaling of the simulated transport fields by the factor β that succeeds in producing a smaller rms difference than is obtained straightaway with $\beta = 1$. When the simulated transports are multiplied by a scale factor $\beta \geq 1.2$, or $\beta \leq 0.8$, there is a marked decrease in the percent variance accounted for, and on this basis we conclude that the hurricane stress fields used in these simulations are consistent with the observed ocean transport to within about 20%.

It remains that there could be a distortion of the stress field that is largely cancelled by averaging over the ensemble of observations. Indeed there is an intriguing hint that the transport difference may not be completely random in that the only large errors seem to occur in the left rear quadrant of the hurricane. By overlaying the observed and simulated transports one can see that the largest difference is found at the position of Norbert AXCPs 3, 20 and 21, and Josephine AXCPs 2, 3, and 4 (Figure 3). In the latter case, satellite imagery shows that pre-hurricane thermal variability was present and may have had associated currents that confound our attempt to interpret the total

signal as if it were hurricane-driven (the rationale for omitting these AXCPs from the statistics in Table V). There is no similar known feature in the Norbert case, however, and so this might also be the result of a sub-hurricane scale stress perturbation not accounted for in these simulations. Whether this is due to non-stationary surface wave effects or to some unresolved variation in the hurricanes wind fields is something that we can not tell from these data alone.

5.2 SML Current

The field of the layer-averaged SML current (Figure 5) looks very much like the transport, and indeed all of the previous discussion of horizontal structure applies equally well here. As we implied in that discussion, the SML current is a near-inertial motion having a small blue shift of frequency. The clockwise turning of the current is most apparent in the Gloria case where the AXCP data span the greatest distance along the track. The wavelength along the track is the inertial wavelength, $U_h \times IP(1-\nu)$, where IP is just the local inertial period, and ν is the blue shift of frequency, typically $\simeq 0.1$ (Price, 1983). These data sets are some of the few ever made that show the horizontal structure of a near-inertial current (see also D'Asaro (1989) and Pollard (1980)).

The SML current simulation by the 3-D model appears fairly realistic in each of the cases, and certainly the large-scale structure of the current field is reproduced quite well. The reasonably good comparison between the simulated and observed currents encourages us to think that the simulated current field can be used as an interpolator between the discrete AXCP data points. It would appear that the AXCP sampling, though less than we had intended, nevertheless does succeed in defining the overall structure of the forced stage response of the SML current.

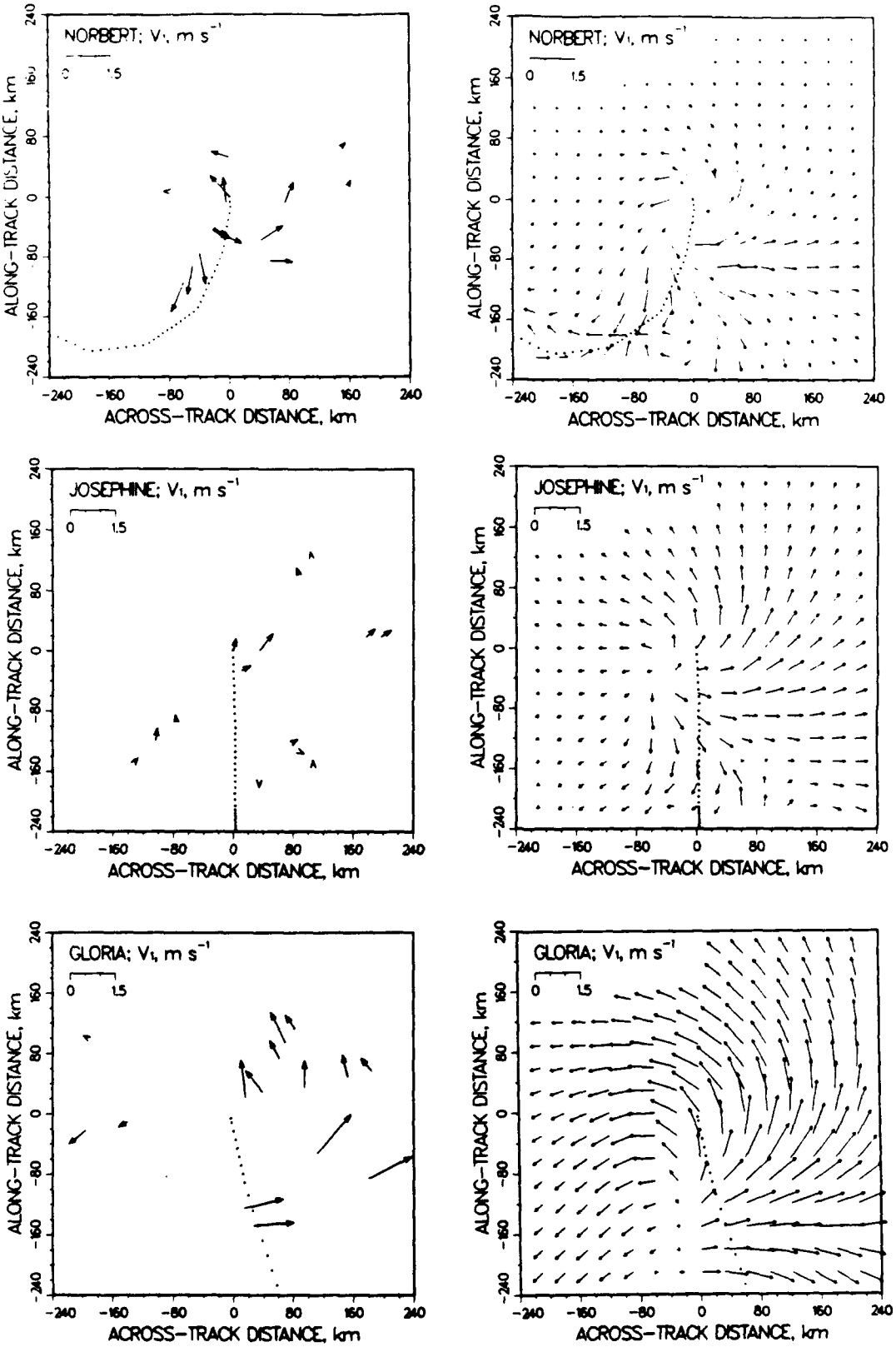

Figure 5. Current vectors within the SML. Note that the qualitative pattern is very similar to that of he transport, and that the largest currents are to the right of the track by about 25 km (Norbert) to 100 km (Gloria).

A close look at the current field shows that it differs from the transport in having not quite such a strong rightward bias in amplitude. This reduced asymmetry arises in the 3-D model solution because enhanced mixing on the right side of the track causes the SML depth to be somewhat greater on the right side of the track, and because, for a given transport, the current amplitude is inversely proportional to SML depth. As we will see in the next subsection, there is also evidence directly from the data that upper ocean mixing is indeed enhanced on the right side of the track.

The statistical comparison between the observed and the simulated current (Table IV) is about as before for the transport. The 3-D model can account for about 80% of the variance in the observed layer-averaged SML currents. The rms difference between the simulated and observed currents is approximately 0.35 m s^{-1}, or not much larger than expected from the total uncertainty on the observations (about 0.3 m s^{-1} overall) (see remarks in Section 3).

Because one goal of this work was to observe the maximum currents produced by the hurricanes, the flight plans included somewhat heavier AXCP sampling over the right side of the tracks. A qualitative comparison between the observed and simulated fields suggests that the AXCP sampling probably did suffice to observe the strongest or very nearly the strongest currents beneath each of these hurricanes. The maximum observed current varied by a factor of almost 2 over these three cases. In the Norbert case the observed (simulated) maximum current was 1.10 (1.11) m s^{-1}, in Josephine it was 0.77 (0.79) m s^{-1}, and in Gloria it was 1.70 (1.38) m s^{-1}. The maximum current increases with both the intensity and size of the hurricane (and model studies suggest dependence upon other external parameters as well (Price, 1981; Greatbatch, 1984)).

5.3 Upper Ocean Mixing

While we argued in Section 4 that the transport is nearly model-independent, the same is not true for the SML current, the SML depth and SML cooling. Each of these is affected significantly by turbulent vertical mixing, which has to be parameterized in any model. If vertical structure is represented by layers, as in our 3-D model, then vertical mixing may be represented by SML entrainment, which has been parameterized in a variety of ways (e.g., the hurricane response models of Elsberry et al. (1976) and Chang and Anthes (1978) give plausible results using a form which is quite different from the one used here). The AXCP data offer a chance to make at least a consistency check on the mixing parameterization of the 3-D model.

5.3.1 SML Depth

When comparing the layered model with oceanic observations, we have to keep in mind that there is a thick transition layer which is a part of the directly wind-driven layer extending well below the literal mixed layer into the stratified fluid below. In the AXCP analysis the transition layer is represented by layer 2 (Appendix). Accordingly, when evaluated from the AXCP data, an equivalent (to a layered model) SML depth (or thickness of the wind-driven layer) is estimated to be $h_1 + h_2/2$, where h_2 is the transition layer thickness (Figure 6).

There is an appreciable small scale variability in the estimates of the SML depth; for example a 16 m difference between neighboring AXCPs 3 and 21 from Norbert. This could be due to real horizontal variations associated with internal waves, or it could also be a result of uncertainty in estimating the transition layer thickness in the AXCP profiles. In either event, the estimated, observed SML depth is a somewhat noisy variable. There is a fairly clear cut trend for SML depth to increase from front to rear. The deepest observed SML value was 62 m at AXCP 13 to the right rear of the

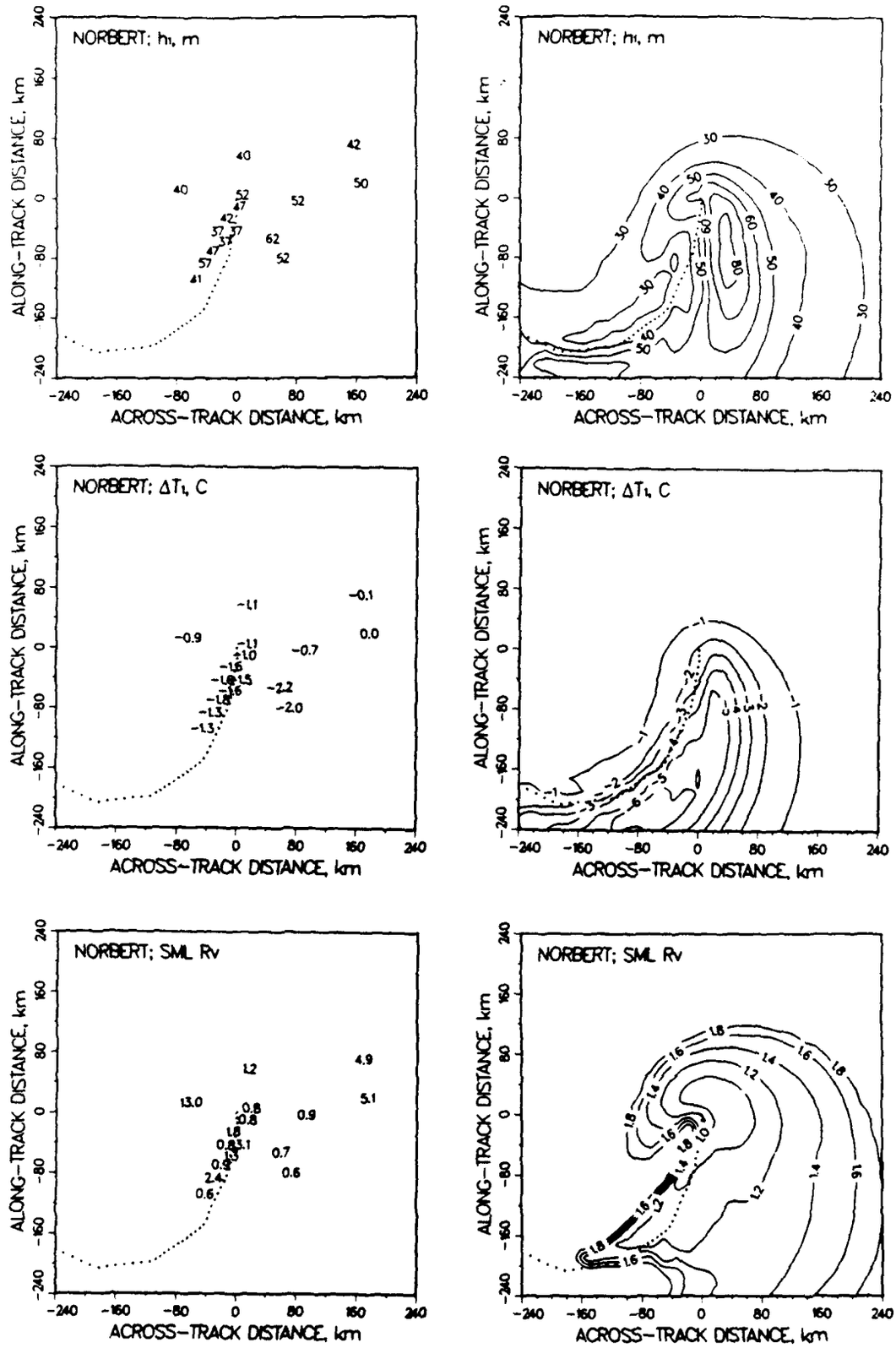

Figure 6. SML depth (top two panels), cooling (middle two panels) and bulk Richardson number (bottom most panels) for the Norbert case. Note that the largest cooling found in the simulation occurs to the rear of the hurricane, and between two AXCP sections.

center. At the same point the 3-D simulation gives a depth of about 70 m, or somewhat deeper. Within the region of greatest mixing to the right of the track, the simulated SML depth roughly doubled during the passage of Norbert.

5.3.2 SML Cooling

The SML cooling (or SST cooling) caused by a hurricane is due almost entirely to vertical mixing (Price, 1981; Cornillon et al., 1987), and should be a particularly sensitive diagnostic of vertical mixing. To evaluate the cooling from this kind of one-time survey data, we have no recourse but to subtract away an estimate of the presumably uniform pre-hurricane surface temperature evaluated as part of the initial condition (Section 3, Table IV). The so-called cooling evaluated in this way is perhaps better described as a temperature anomaly, and we noted already in Section 3 that it gives a very muddled picture of the cooling response to Josephine and Gloria.[1] Thus we limit this discussion to the Norbert data set, which apparently had much weaker pre-hurricane variability.

In the Norbert case there is at least a clear trend for cooling to increase from front to rear (Figure 6), which must obtain if the cooling is due to the hurricane. It appears that there is some rightward asymmetry of cooling with the greatest values of about 2.2 C to the right of the track. The simulation gives roughly comparable values at the

[1]Cornillon et al. (1987) have reported satellite infrared images of the western North Atlantic that provide a remarkable view of the sea surface cooling caused by hurricane Gloria. By differencing pre- and post-hurricane images, they were able to isolate clearly the SST cooling effect of the hurricane. Gloria caused pronounced cooling along a track extending from the subtropics all the way north to New England. Over the Sargasso Sea, the maximum cooling was found about 100 km to the right of the track, or roughly where we find the maximum SML current and maximum cooling response in our models (1-D or 3-D) (Figures 4 and 5).

AXCP positions, but also suggests that larger cooling might have taken place behind the hurricane where observations were not taken.

Overall, these comparisons of SML depth and cooling are rather unconvincing, partly because we can see a reasonably clear mixing signal in only one of three cases, but partly too because the AXCP sampling for these variables appears not to have been as apt as it was for SML current and transport.

5.3.3 Bulk Richardson Number

In both models the mixing effect of wind-driven currents is parameterized by a function of a bulk or a gradient Richardson number (3-D or 1-D respectively) that predicts steeply increasing mixing as the Richardson number is forced below a quasi-'critical' value. The idea of a critical *gradient* Richardson number control on mixing is well established (e.g., Mellor and Yamada, 1982); the equivalent for the bulk Richardson number is much less so. The parameterization used here, Eqn. (1), gives significant entrainment when R_v is less than 1, and very small entrainment for R_v greater than 1. If this were indeed appropriate, then we should observe that R_v is somewhat less than 1 in regions of strong mixing, and that R_v should always be larger than 1 where mixing is very weak or vanishing.

To evaluate R_v from the AXCP data we estimate the density difference to be $\delta\rho = \alpha\delta T$, where δT is the temperature change across the transition layer (listed in Table 1 of the Appendix), α is the thermal expansion coefficient (-0.32 kg m^{-3} C^{-1}), the SML thickness is estimated as noted above, and the current difference is estimated to be $\delta \boldsymbol{V} = \boldsymbol{V}_1 - \boldsymbol{V}_3$, where $\boldsymbol{V}_3$ is the thermocline current. In profiles where the SML current is large (greater than about 0.5 m s^{-1}) there is generally a well-defined transition layer with a clear δT. In such profiles R_v is then well defined from the field data. However, at locations where the SML current is small (left of the track and ahead of the eye) there

is only a thin and sometimes indistinct transition layer, and consequent uncertainty in estimating δT. As a result, the R_v evaluated from the AXCP data is then rather uncertain, and we suspect probably overestimated in regions where it would have been large (compared to 1) anyway.

The smallest R_v are found to the right of the track and just behind the eye where entrainment is expected to be strongest (Figure 6). Typical values in this region are in the range 0.5 to 1.0, which are not inconsistent with the expectations from the entrainment parameterization. Larger values, which are in some cases very uncertain owing to uncertainty in the temperature change and depth limits of the transition layer, are found in regions to the left of the track, and ahead of the hurricane where entrainment is weak or nearly vanishing. Indeed, all of the R_v estimates in these outlying regions are large compared to 1. Thus the observed, bulk Richardson number has a pattern underneath the hurricane which is at least roughly consistent with the entrainment parameterization used in the 3-D model.

A similar pattern obtains also for the Josephine and Gloria cases. An intriguing difference in detail is that the smallest values of R_v are slightly larger in the Josephine case, about 1.0, and are slightly smaller in the Gloria case, as low as 0.5. The 3-D model on the other hand, tends to give somewhat more evenly distributed small values. This may be evidence that while a form something like our Eqn. (1) is appropriate for these kinds of problems, there may not be quite such a steep roll-off with increasing R_v as suggested by (1) (i.e., the exponent may be less than 4).

6 Thermocline Currents

An important and somewhat surprising result of this study is the observation of substantial thermocline-depth currents under the rear half of hurricane Norbert, Fig-

ure 7. This is evidence of an unusually strong pressure-coupling between the SML and thermocline in that case, and consistent with the comparatively large SML Burger number, $M = 0.5$. These large thermocline currents show that in the Norbert case the forced stage response and the relaxation stage response overlapped in time, and that non-local dynamics were likely to be important during the forced stage response. (There is a somewhat weaker coupling in the other two cases as well, but the thermocline-induced currents are apparently obscured by ambient currents; evidence of this is stronger thermocline-depth currents under the leading edge of hurricane Gloria than behind it.)

The 3-D model gives a plausible simulation of the thermocline current, and helps to show the mechanism of pressure-coupling via inertial pumping (see also Shay et al., 1989, who model the deep response by a summation of normal modes). With some guidance from the simulation it is easy to see that the SML current field (Figure 5) is strongly divergent in a region just behind the hurricane; the current to the right of the track flows to the right with a large amplitude, while the current to the left of the track flows away from the track but is much weaker. This divergence acts to compress the SML and to upwell the thermocline. Because the SML current oscillates with a near inertial period, so too does the divergence and the associated up- and downwelling, which has been termed 'inertial pumping' (Price, 1983). The area shown in Figure 7 covers a little less than one day of time along the track, and so we see only the first cycle of the inertial pumping. Because Norbert was intense and comparatively small, the inertial pumping had a large amplitude, the simulations suggesting that $\eta \approx 40$ m at maximum, or more than half the SML thickness. The largest upwelling seen in the data was about 25 m, but the simulations suggest that larger upwelling (and currents) may have occurred just behind the hurricane in an area not sampled by AXCPs.

The dynamical effect of the inertial pumping is to produce a hydrostatic pressure perturbation within the SML and the main thermocline. The region of upwelling just behind the hurricane center causes a low pressure perturbation whose amplitude in

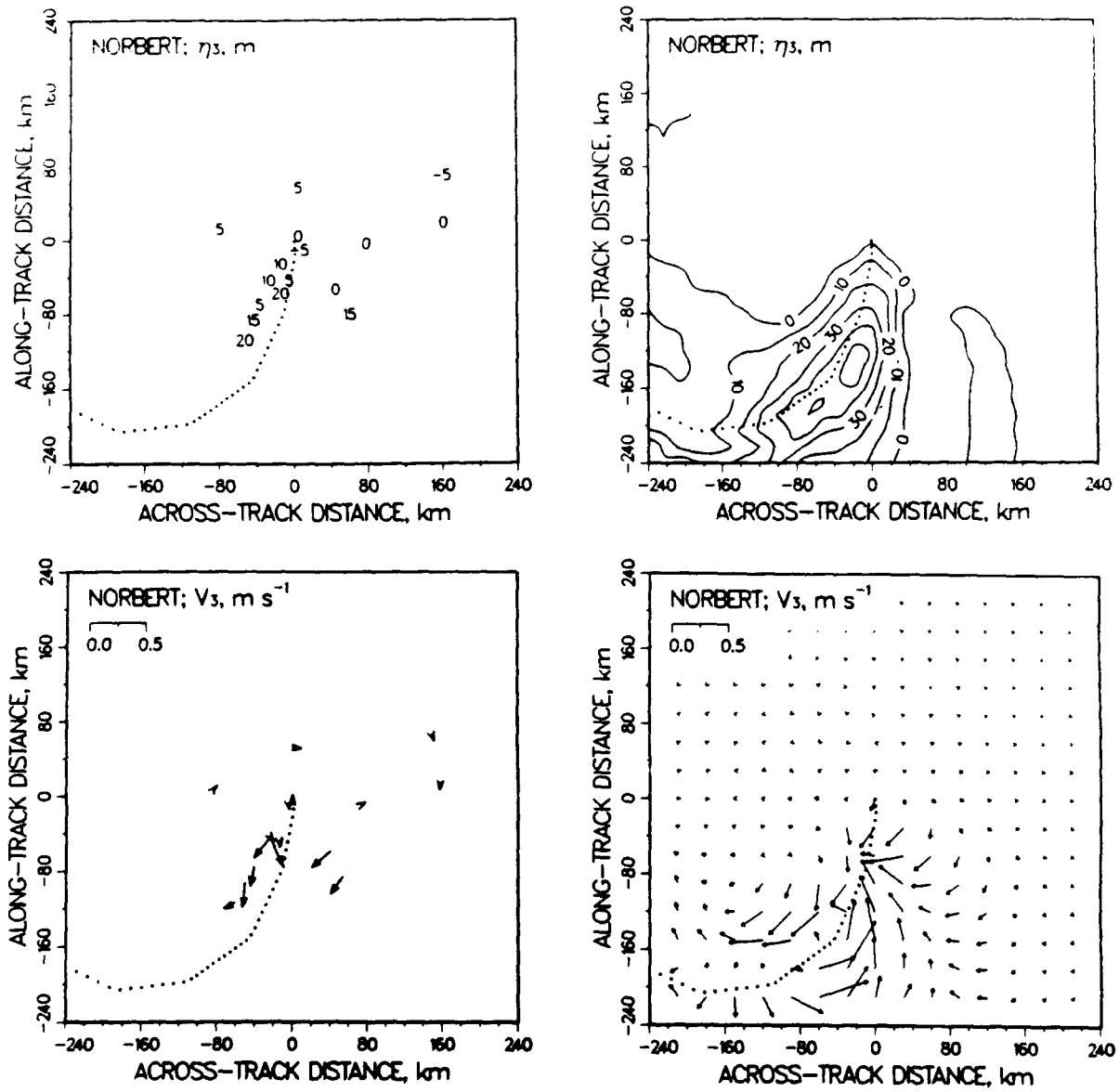

Figure 7. Upwelling (top two panels) and thermocline-depth current (bottom two panels) from Norbert. The maximum upwelling in the simulation (top right panel) occurs just between the AXCP sections made behind the hurricane.

the SML or upper thermocline is approximately $g' \eta \rho$, and decreasing with depth in the thermocline (Table III shows how η depends upon external parameters). The horizontal scale of η is roughly 3 R_{max} (Figure 7), and thus the thermocline is accelerated toward the upwelling maximum which occurs just behind the hurricane center. The amplitude of the acceleration is $A \approx \frac{g' \eta}{3 R_{max}} \approx 2.5 \times 10^{-5}$ m s^{-2} (see Fig. 7 of Price (1983) for the horizontal structure). This acceleration oscillates in time along with the inertial pumping, and so the resulting thermocline currents also have a near-inertial time dependence, which is apparent in Figure 7 (lower panels) as a clockwise turning with increasing distance behind the hurricane center. The maximum amplitude of the thermocline currents is roughly the time integrated acceleration over the first half inertial period, or, $A \times 2 \times 10^4$ s ≈ 0.5 m s^{-1}, which is an appreciable fraction, ≈ 0.4, of the SML current (this fraction being proportional to and nearly equal to the SML Burger number). Note that the thermocline-depth currents have a rather complex and small scale horizontal structure compared with the very simple pattern of either the SML current or of the upwelling itself, since they are forced by the horizontal gradient of the pressure.

The vertical structure of the thermocline response is also very simple during at least the early part of the relaxation stage that we see here. The inertial pumping has a nearly uniform phase and amplitude through the thermocline; the pressure perturbation has the same phase but decreasing amplitude with increasing depth. The thermocline currents forced by this pressure perturbation should have just the same vertical structure, and clear evidence of this appears in Norbert AXCPs 13 and 20, which have the largest thermocline currents (Figure 8). They show a very simple structure in the thermocline, with nearly uniform phase and decreasing amplitude with depth. Note though that the phase difference between the SML current and the upper thermocline current can be 180 degrees, as in AXCP N13, or nearly zero as in N21.

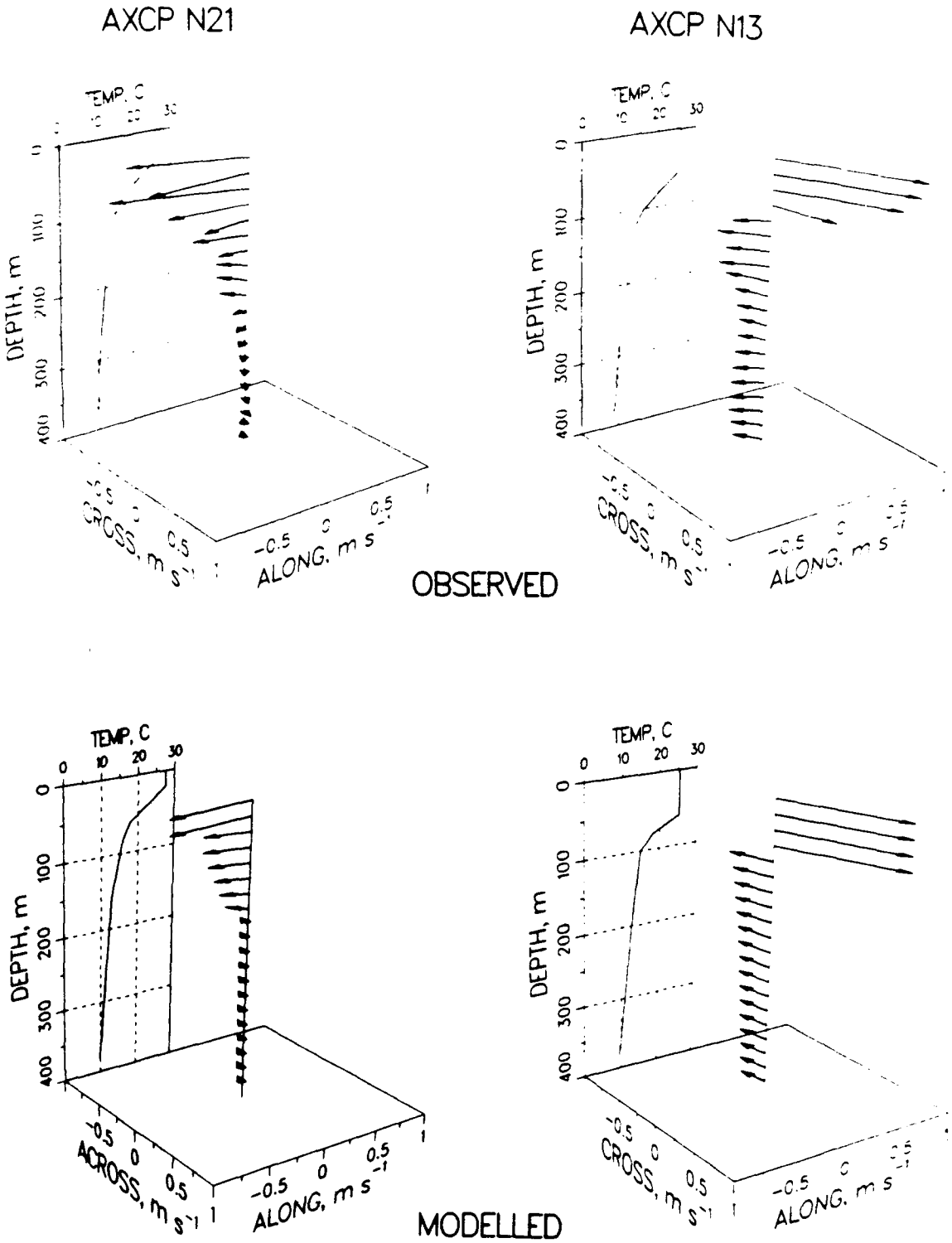

Figure 8. Current and temperature profiles from Norbert AXCP 21 (upper left) and AXCP 13 (upper right). These profiles were taken to the left and right of the track (see Figure 3). In this figure only, the AXCP data are shown in a nearly raw form; the only data processing being a simple boxcar smoothing over a roughly 10 m interval. The surface wave component has not been removed, but was fairly small in both profiles. The bottom two panels are the model-simulated current and temperature at the locations of AXCP 20 and 13. Note that the upper thermocline current (depths below 70 m) has an appreciable amplitude, and only small phase change with depth.

This very simple vertical structure can be simulated by a model having only a few active thermocline layers (compare the simulated current profiles in Figure 8 (lower) with the observed profiles above). Indeed, a model having only *one* active thermocline layer can simulate the vertical phase, near-inertial time-dependence, and the thermocline-averaged amplitude of the initial relaxation stage response. However, as the relaxation stage response continues to develop during the next several days to weeks, this structure will become somewhat more intricate (Price, 1983). Brink (1989) has observed the thermocline depth currents in the Gloria case in moored array data, and noted that the phase change across the thermocline grew to more than half a cycle within about a week after the hurricane passage. To simulate this structure without serious error requires more vertical resolution than is given by one or a few layers.

In the Norbert case the observed thermocline currents were up to 0.3 m s^{-1} directly under the hurricane, and model results suggest that stronger currents may have occurred in a region behind the hurricane that was not sampled by AXCPs. The energy and momentum of these thermocline currents comes from the wind-driven SML current by the mechanism of inertial pumping and pressure-coupling described above, and this process causes the SML current to decay in time with an e-folding scale of typically 5 days (Price (1983); this is the process often parameterized in 1-D models by a linear drag, see for example Pollard and Millard (1970) who first described this). If the pressure coupling is arbitrarily suppressed in the 3-D model, then the simulated maximum SML current in the Norbert case changes considerably, increasing by about 35%. Thus the non-local dynamics of the relaxation stage response were important even during the forced stage response to Norbert (or more to the point, in a case with Burger number, $M \geq \frac{1}{2}$).

7 Vertical Shear Within the Surface Mixed-Layer

In this section we examine the vertical shear of the SML current, and compare AXCP profile measurements with simulations of the current made by the 1-D model. In Part I we discussed at length the problem of separating the observed current measured by AXCPs into surface wave, shear and layer average mean currents. In brief, we found that the fitting procedure used to analyze the profiles gives very reliable estimates of the layer-averaged mean current; sensitivity studies showed that bias of the estimated mean SML current was 0.02 m s^{-1} and that the coefficient of variation was 0.07. The vertical shear of the SML current was found to be more difficult to estimate because the change in wave amplitude with depth can be aliased to appear as shear, especially when the SML is shallow and only one or fewer wave cycles are sampled within the SML. The coefficient of variation for the estimated shear in the SML was thus very high, 1.02, but the bias was only -0.0004. In comparing the shear estimated from the AXCP measurements with the simulations from the 1-D model, we can thus expect that the scatter of individual estimates will be very large even if the model were perfect, but that the mean value and mean trend over an ensemble of estimates should be useful for verifying the model.

Figure 9 shows the measured and simulated profiles of current magnitude for AXCP 27 from Gloria. The layer averaged SML current in this profile was 1.70 m s^{-1}, which was the largest SML current measured in the three storms. The shear in the SML was more or less aligned with the mean current, and was about 0.01 s^{-1}. Hence, the estimated surface current in this profile was 2.04 m s^{-1}. The shear in this profile is thus a significant feature for many design studies. Note that the shear in the transition layer is only slightly larger than the shear in the mixed layer for this profile. More typically, the shear in the stratified transition layer is considerably larger than is the shear in the SML.

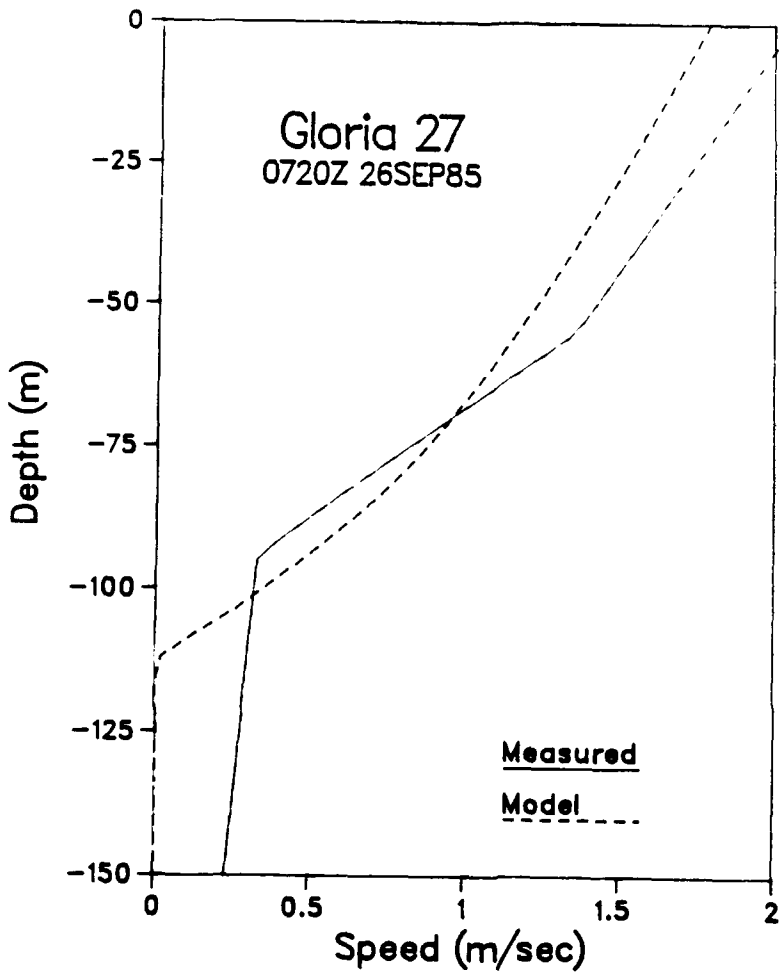

Figure 9. Profile of current speed measured at Norbert AXCP 27 (solid line), and as simulated by the one-dimensional boundary layer model (dashed line).

The current profile from the 1-D model simulation is shown as the dashed line in Figure 9. Within the SML and transition layers the simulated shear is very similar to that observed (in the 1-D model there is no current below the transition layer since there is no pressure coupling with the thermocline.) In this and in many cases, the overall depth of vertical mixing, as judged by the thickness of the wind-driven layer, is reasonably consistent between the 1-D model simulation and the observations.

A scatter plot of simulated vs. measured SML shear in the direction of the local, flight-level wind is given by Figure 10, which includes all three cases. The simulated shear was estimated from the 1-D model results by a fitting procedure much like that applied to the AXCP data. The solid circles indicate flight level winds less than 30 m s^{-1}, and the open circles indicate weaker winds. The scatter in the plotted points is very large, but expected from the uncertainty in the fit to the measured profiles (the coefficient of variation between the measured and simulated shears is about 1, or comparable to the coefficient of variation found in the sensitivity studies of Part I). The same data are also shown in Figure 11, where measured shear values are open circles, and simulated shear values are asterisks. The solid and dashed lines are averages over 10 m s^{-1} ranges of wind speed for the measured and simulated shears respectively. Note that there are some estimates from both the data and the model indicating a shear that is opposed to the local wind. These arise from cases where there has been a rapid change in wind direction, and indicate that the shear and the wind stress are not in a steady state.

Despite the scatter and the nonstationary effects, there is a clear trend for shear to increase with wind speed in both the observations and the 1-D model results. At moderate wind speeds, ≤ 20 m s^{-1}, the shear is roughly 0.03^{-1}, and is somewhat overestimated by the model. At the largest wind speeds, up to 40 m s^{-1} which corresponds to a stress of about 4 Pa, the measured shear is roughly 0.01 s^{-1}, and is simulated well by the 1-D model. A shear of this magnitude can be significant for some purposes,

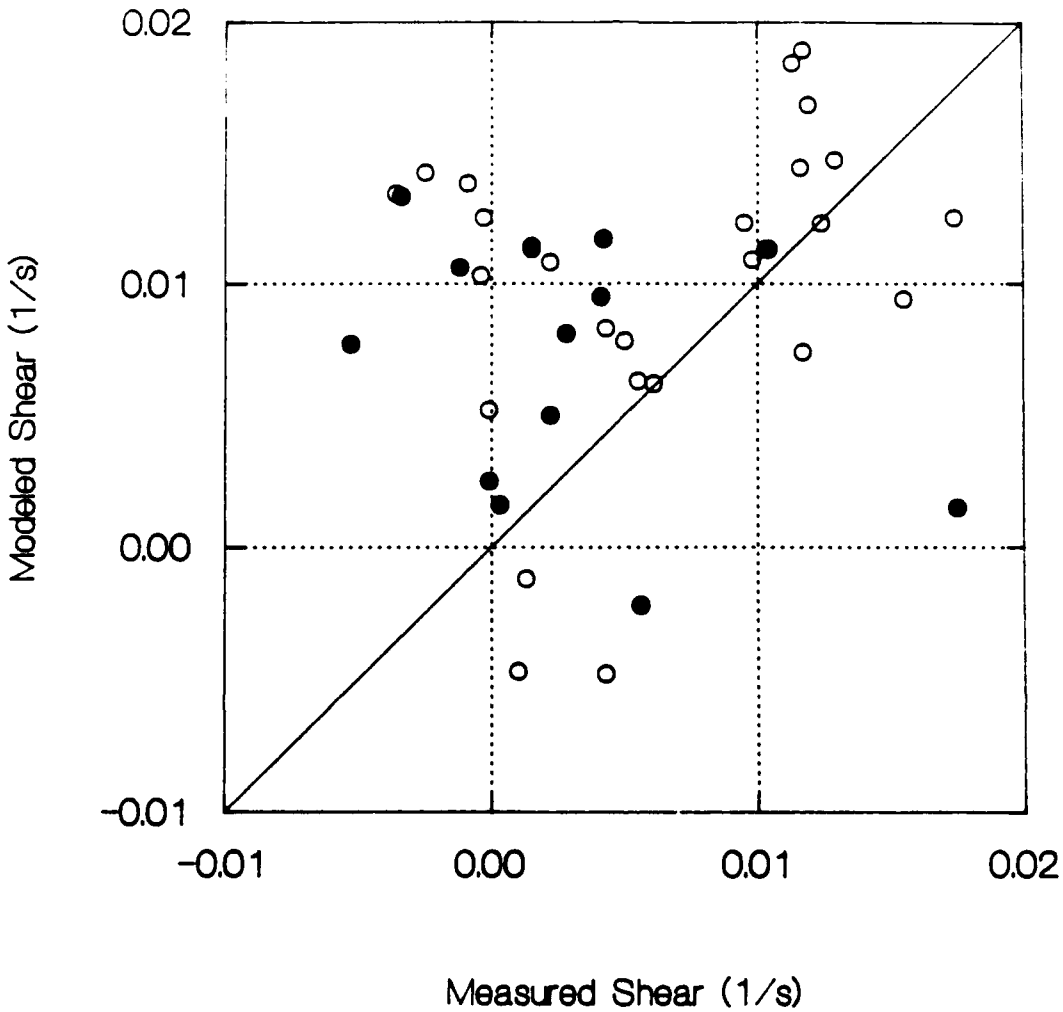

Figure 10. Vertical shear of the SML current in the direction of the local wind. 1-D simulated values are plotted against measured values. The open circles indicate estimates made where wind speed was greater than than 25 m s^{-1}, solid circles are estimates at all lower wind speeds.

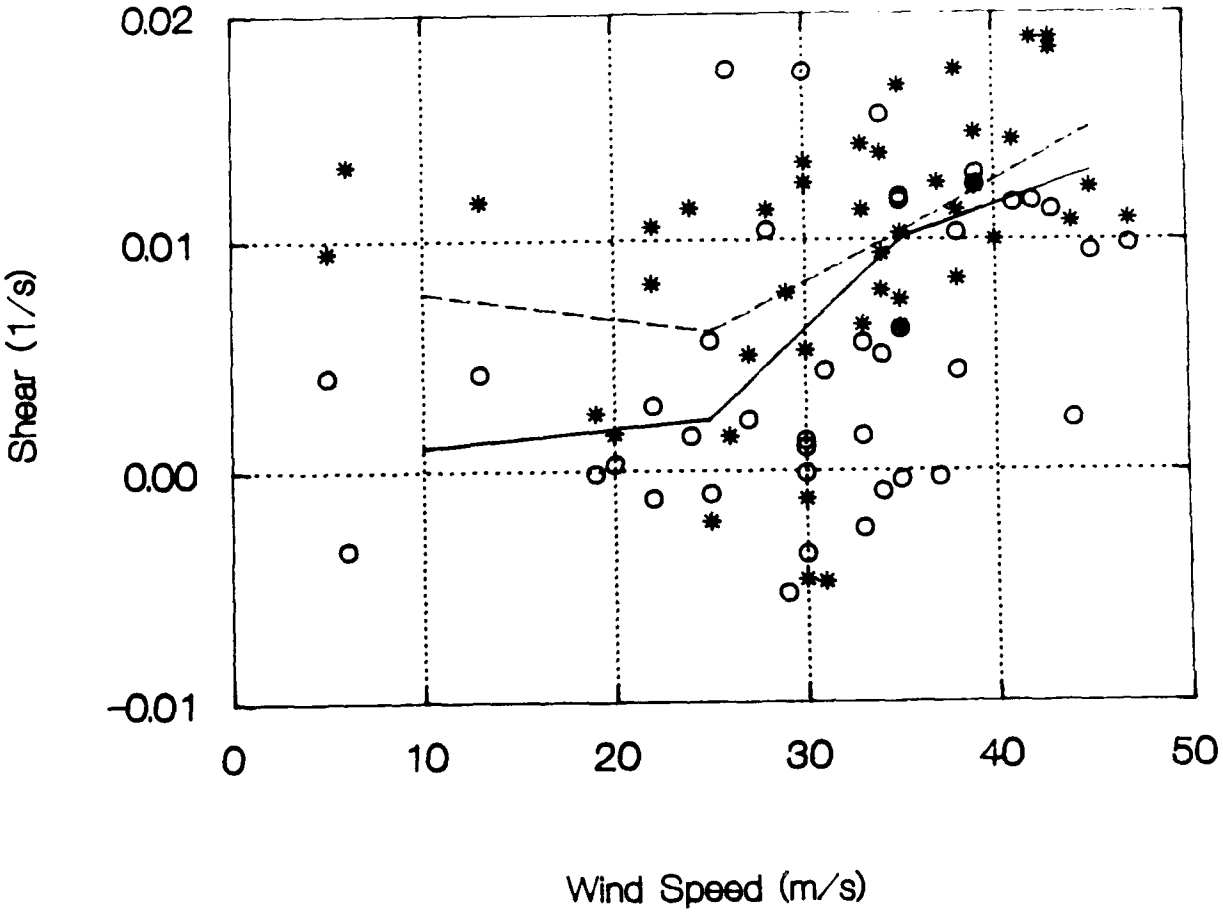

Figure 11. Vertical shear of the SML current as a function of wind speed. Open circles are estimates made from AXCP data, and asterisks are estimates made from the 1-D model simulations. Solid and dashed lines are average trends computed from the observations and simulations respectively.

and specifically, it shows that a correct layered model would tend to underestimate the surface currents by about 0.2 m s^{-1} in hurricane conditions.

8 Summary and Remarks

We believe that the most important result of this study and Part I is the demonstration that useful observations of ocean currents can now be acquired under the most extreme weather conditions, and that numerical ocean models are able to rationalize the main features of such data sets. Our practical goal, to observe and model storm-driven currents for design purposes, appears to be within reach, at least for open ocean conditions.

The scientific goals for this work were somewhat more open-ended, but we hope partially realized here by showing how the horizontal structure of the forced stage SML response is imposed by the atmospheric forcing due to the hurricanes. If a storm has a non-dimensional speed S of O(1), as these and most hurricanes do, then the dominant horizontal structure of SML currents can be understood as the local response of the ocean to a time variable wind stress. At locations where the stress turns in the sense of an inertial current (right side of the track), the response can be greatly enhanced. The across-track scale of the response is the scale of the hurricane, and the along-track scale is just the product of the storm translation speed and the inertial period. The vertical structure of the forced stage response is also quite simple. The wind-driven SML current has a fairly small vertical shear, typically 0.01 s^{-1} under very high stress conditions, which may nonetheless be important for some design purposes. Most vertical shear occurs within a stratified transition layer which has a thickness roughly half that of the SML.

In the Norbert case, which is characterized by a fairly large SML Burger number, we can see the start of the relaxation stage response; appreciable upwelling and thermocline-depth currents occurred beneath the trailing edge of the hurricane. These thermocline-depth currents also have a simple vertical structure, having very little phase change with depth and a monotonically decreasing amplitude. Their horizontal structure is more complex, but is directly related to the horizontal structure of the forced stage response through the field of inertial pumping and hydrostatic pressure perturbation.

Several specific modeling questions were raised in this study, and were addressed by comparison of model simulations with the observations. First, we found that for the purpose of modeling ocean currents the hurricane wind stress fields can be estimated well from conventional methods. Sub-hurricane scale errors may be present (in the left rear quadrant), but are not readily identified in these data sets. Second, we found that the bulk Richardson number estimated from AXCP data takes on values just less than 1 in regions near the hurricane center where vertical mixing was expected to be strongest, and is larger in outlying regions. This is consistent with a Richardson number closure for mixing. Third, we noted here and in Part I that the forced stage response and the early relaxation stage response have a very simple vertical structure that can be represented by a layered model. If the Burger number is appreciable (as in the Norbert case), a 3-D model having the dynamics of inertial pumping seems necessary, even for the forced stage response. Fourth, the high resolution 1-D model was found to give useful simulations of the SML current vertical shear, especially in the range of very large wind speed where the vertical shear is largest and most important.

These data sets show the great power that aircraft-deployed expendable instruments can bring to studies of air/sea interaction. Aircraft can provide oceanographic sampling in definite relationship to synoptic weather, and at the same time provide a high quality view of the winds. However, our problems with interpretation of the

Sargasso Sea data sets should be a caution to future investigators that one-time survey data will not always be sufficient to sort out storm-induced currents from ambient currents. In future studies it would be useful to acquire initial survey data, and just as important and perhaps more effective, avoid regions of high ambient variability. The AXCP sampling plan employed in these studies appears to have sampled the SML currents fairly well, especially the regions of strongest current. Sampling within the thermocline appears to have been less satisfactory, and could be easily improved in future studies by making a section across the hurricane track and about 100 km behind the hurricane center.

Acknowledgments

The field programs that made this study possible were supported by a Joint Industry Program entitled Ocean Response to a Hurricane; corporate members were Amoco Production Co., Arco Oil and Gas Co., Chevron USA Inc., Conoco Inc., Exxon Production Research, Gulf Oil Exploration and Production Co., Marathon Oil Co., Mobil Research and Development Co., Shell Development Co., and Sohio Petroleum Co. Guidance and encouragement were provided by a technical committee chaired by James Haustein; members were Gene Berek, Thomas Mitchell, James Allender, Robert Gordon, David Peters, Michael Feifarek, Irving Brooks, and Sherman Chiu. The authors are grateful to all of those who participated in the technical developments and flight operations which made the measurements possible. Field operations and program management were conducted by James Feeney of Horizon Marine, assisted by William Kucharski and Jennifer Briggs. Development of AXCP hardware was carried out by Robert Drever of the University of Washington Applied Physics Laboratory. Flight operations were supervised by Peter Black of the NOAA Hurricane Research Division and Jan Zysko of the NOAA Office of Aircraft Operations. JFP and TBS were supported

by the Office of Naval Research during the period of manuscript preparation (JFP by grant no. N00014-89-J-1053).

References

Black, P. G., 1983: Ocean temperature changes induced by tropical cyclones. Ph.D. dissertation, The Pennsylvania State Univ., 278 pp.

Black, P. G., R. L. Elsberry, L. K. Shay, R. Partridge, and J. Hawkins, 1988: Hurricane Josephine surface winds and ocean response determined from air-deployed drifting buoys and concurrent research aircraft data. *J. Oceanic Atm. Tech.*, **5**, 683–698.

Brooks, D., 1983: The wake of hurricane Allen in the western Gulf of Mexico. *J. Phys. Oceanogr.*, **13**, 117–129.

Brink, K. H., 1989: Observations of the response of thermocline currents to a hurricane. *J. Phys. Oceanogr.*, **19**, 1017–1022.

Cardone, V. J., A. J. Broccoli, C. V. Greenwood, and J. A. Greenwood, 1980: Error characteristics of extratropical storm wind fields specified from historical data. *J. Petrol. Tech.*, **32**, 873–880.

Cardone, V. J., and D. B. Ross, 1979: State-of-the-art wave prediction methods and data requirements. *Ocean Wave Climate*, edited by M. D. Earle and A. Malahoff. Plenum Publishing Corp., pp. 61–91.

Chang, S. W., and R. A. Anthes, 1978: Numerical simulations of the ocean's nonlinear, baroclinic response to a moving hurricane. *J. Phys. Oceanogr.*, **8**, 468–480.

Church, J. A., T. M. Joyce, and J. F. Price, 1989: Current and density observations across the wake of Typhoon Gay. *J. Phys. Oceanogr.*, **19**, 259–265.

Cooper, C., and J. D. Thompson, 1989a: Hurricane-generated currents on the outer continental shelf Part 1: Model formulation and verification. *J. Geophys. Res.*, **94**, 12,513–12,539.

Cooper, C., and J. D. Thompson, 1989b: Hurricane-generated currents on the outer continental shelf Part 2: Model sensitivity studies. *J. Geophys. Res.*, **94**, 12,540–12,554.

Cornillon, P., L. Stramma, and J. F. Price, 1987: Satellite measurements of sea surface cooling during hurricane Gloria. *Nature*, **326**, 373–375.

D'Asaro, E. A., 1989: The decay of wind-forced mixed layer inertial oscillations due to the β-effect. *J. Geophys. Res.*, **94**, 2045–2056.

Elsberry, R., T. Fraim, and R. Trapnell Jr., 1976: A mixed-layer model of the oceanic thermal response to hurricanes. *J. Geophys. Res.*, **81**, 1153–1162.

Forristall, G. Z., R. C. Hamilton, and V. J. Cardone, 1977: Continental shelf currents in Tropical Storm Delia: Observation and theory. *J. Phys. Oceanogr.*, **7**, 532–546.

Forristall, G. Z., E. G. Ward, V. J. Cardone, and L. E. Borgman, 1978: The directional spectra and kinematics of surface waves in Tropical Storm Delia. *J. Phys. Oceanogr.*, **8**, 888–909.

Frank, W. M., 1977: The structure and energetics of the tropical cyclone I, Storm structure. *Mon. Wea. Rev.*, **105**, 1119–1135.

Geisler, J. E., 1970: Linear theory on the response of a two-layer ocean to a moving hurricane. *Geophys. Fluid Dyn.*, **1**, 249–272.

Gill, A. E., 1984: On the behavior of internal waves in the wakes of moving storms. *J. Phys. Oceanogr.*, **14**, 1129–1151.

Greatbatch, R. J., 1984: On the response of the ocean to a moving storm: parameters and scales. *J. Phys. Oceanogr.*, **14**, 59–77.

Large, W. G., and S. Pond, 1981: Open ocean momentum flux measurements in moderate to strong winds. *J. Phys. Oceanogr.*, **11**, 324–336.

Martin, P. J., 1982: Mixed-layer simulation of buoy observations taken during Hurricane Eloise. *J. Geophys. Res.*, **87**, 409–427.

Mellor, G. L., and P. A. Durbin, 1975: The structure and dynamics of the ocean surface mixed layer. *J. Phys. Oceanogr.*, **5**, 718–728.

Mellor, G. L., and T. Yamada, 1982: Development of a turbulence closure model for geophysical fluid problems. *Rev. Geophys. Space Phys.*, **20**, 851–875.

Miller, B. J., 1964: A study of the filling of Hurricane Donna (1960) over land. *Mon. Wea. Rev.*, **92**, 389–406.

NOAA Technical Report NWS 23, 1979: Meteorological criteria for standard project hurricane and probable maximum hurricane wind fields, Gulf of Mexico and east coast of the United States. U.S. Dept. of Commerce, Washington D.C., 320 pp.

Pollard, R. D., 1980: Properties of near-surface inertial oscillations. *J. Phys. Oceanogr.*, **10**, 385–398.

Pollard, R. T., and R. C. Millard, 1970: Comparison between observed and simulated wind-generated inertial oscillations. *Deep-Sea Res.*, **17**, 813–821.

Powell, M. D., 1980: Evaluations of diagnostic marine boundary layer models applied to hurricanes. *Mon. Wea. Rev.*, **108**, 757–766.

Price, J. F., 1981: Upper ocean response to a hurricane. *J. Phys. Oceanogr.*, **11**, 153–175.

Price, J. F., 1983: Internal wave wake of a moving storm. Part I: Scales, energy budget and observations. *J. Phys. Oceanogr.*, **13**, 949–965.

Sanford, T. B., P. G. Black, J. R. Haustein, J. W. Feeney, G. Z. Forristall, and J. F. Price, 1987: Ocean response to a hurricane. *J. Phys. Oceanogr.*, **17**, 2065–2083.

Shay, L. K., and R. L. Elsberry, 1987: Near-inertial current response to hurricane Frederick. *J. Phys. Oceanogr.*, **17**, 1249–1269.

Shay, L. K., R. L. Elsberry, and P. G. Black, 1989: Vertical structure of the ocean current response to hurricanes. *J. Phys. Oceanogr.*, **19**, 649–669.

Stewart, R. W., 1974: The air-sea momentum exchange. *Boundary-Layer Met.*, **6**, 151–167.

Stramma, L., P. Cornillon, and J. F. Price, 1986: Satellite observations of sea surface cooling by hurricanes. *J. Geophys. Res.*, **91**, 5031–5035.

Voorhis, A. D., 1969: The horizontal extent and persistence of thermal fronts in the Sargasso Sea. *Deep-Sea Res.*, **16**(Supplement), 331–337.

Appendix

AXCP Data Tabulations and Analysis Method

a) AXCP Station Data

The P3 aircraft flew a similar, more or less star-shaped pattern through each hurricane (Fig. 1A shows the Gloria flight path). AXCPs were dropped at roughly 25 km intervals, with enhanced sampling on the right side of the track. In each case about 15 AXCPs produced useful data (Table 1A).

The AXCPs measure temperature, and the motionally-induced electric field set up by ocean currents and the orbital motions of surface gravity waves. They fall through the water at a rate $W = 4.5$ m s^{-1} to a depth of 1500 m (fast-fall probes), or at a reduced rate, $W = 2.2$ m s^{-1}, to a depth of 200 m (slow-fall probes). Because of a rapid wind-driven drift of the surface buoy due to very high winds encountered in hurricanes, most of the fast-fall probes produced usable data down to only about 800 m, which is more than adequate for this study.

b) AXCP Analysis

The currents inferred directly from AXCP measurement are relative currents because of an unknown reference, U_r, which is independent of depth. In these experiments we have estimated U_r as the depth-independent current in the deepest portion of the profiles (see Figure 2A for an example). The estimated reference currents were usually less than 10 cm s^{-1}, and their uncertainty is not thought to be significant.

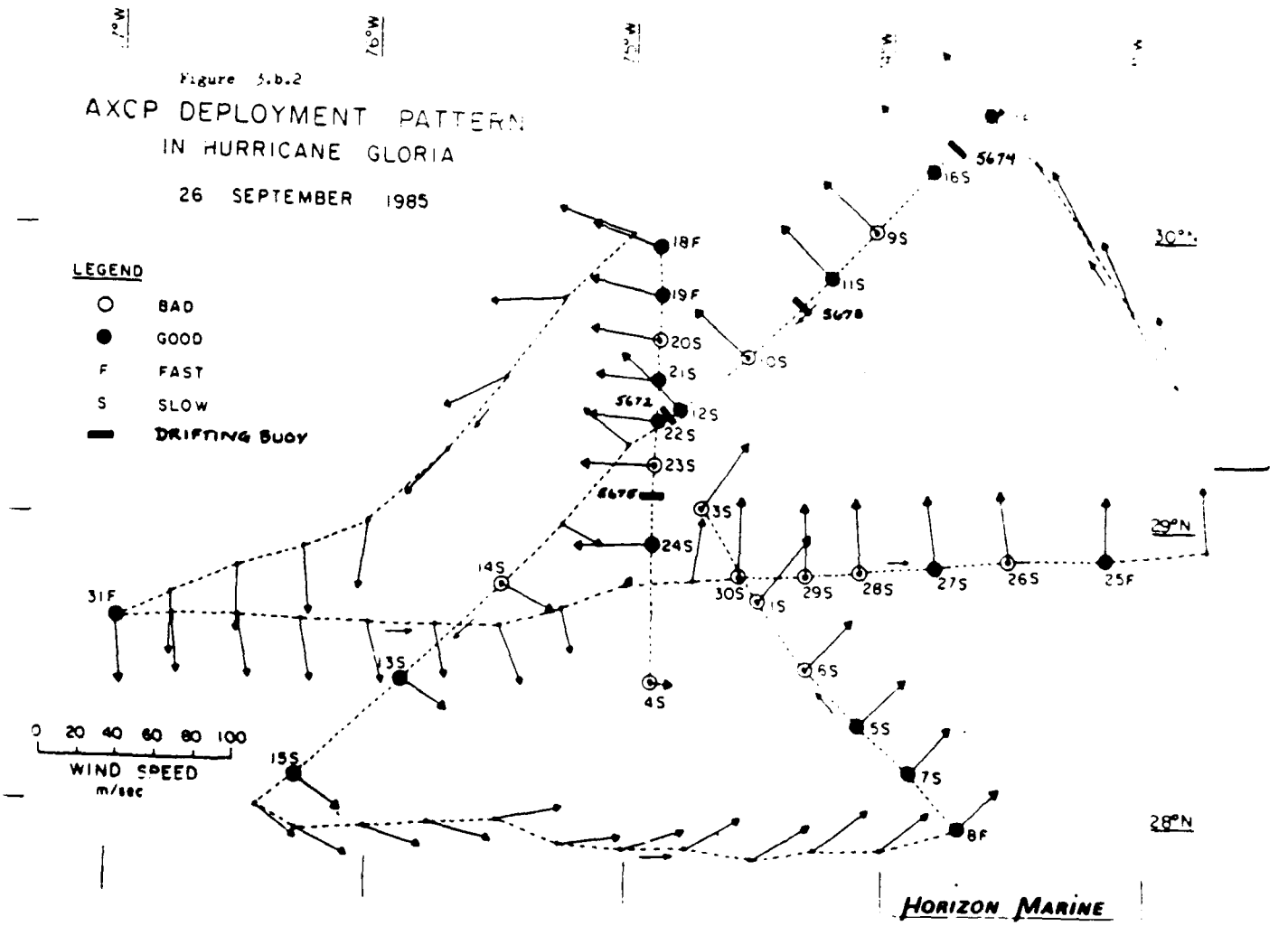

Figure 1A. Flight track and wind observations from hurricane Gloria.

Table 1A: AXCP station data.

D # is the AXCP number; N denotes Norbert, J, Josephine, G, Gloria. F/S indicates fast- or slow-fall probe. X and Y are the along-track and across-track coordinates in the storm-centered system; X increases toward the top of the figure. Y increases to the right. TML is temperature of the surface mixed layer, and δT is the temperature change across the transition layer. η is the apparent upwelling within the thermocline. Z_i is the depth of layer i.
a: AXCP G19 did not go deep enough to measure layer 3.

D #	F/S	lat. deg. N	lon. deg. E	date	time UTC	X km	Y km	TML C	δT C	η m	Z_1 m	Z_2 m	Z_3 m
N 2	F	20.56	-108.20	23SEP84	2244	149.2	65.8	28.4	2.5	-5.	-30.	-55.	-200.
N 3	F	18.11	-108.76	24SEP84	17	-61.5	-113.7	27.2	5.0	20.	-32.	-50.	-200.
N 4	F	20.25	-107.86	23SEP84	2253	157.5	14.4	28.5	3.0	0.	-40.	-60.	-200.
N 6	F	19.60	-108.33	23SEP84	2311	74.0	-8.7	27.8	3.0	0.	-45.	-60.	-200.
N13	F	19.07	-108.31	23SEP84	2335	40.6	-58.5	26.3	5.0	0.	-45.	-80.	-200.
N14	F	18.96	-108.07	23SEP84	2339	53.7	-85.5	26.5	3.0	15.	-40.	-65.	-200.
N15	S	19.41	-109.08	24SEP84	112	0.0	0.0	27.4	5.0	0.	-40.	-65.	-200.
N16	S	19.20	-108.95	23SEP84	2359	-4.6	-8.3	27.5	5.0	-5.	-35.	-60.	-200.
N18	F	18.83	-108.88	24SEP84	5	-23.5	-44.4	27.0	5.0	5.	-30.	-45.	-100.
N20	F	18.51	-108.83	24SEP84	11	-40.7	-75.2	26.7	5.0	5.	-35.	-60.	-200.
N21	F	18.33	-108.80	24SEP84	13	-50.2	-92.2	27.2	8.0	15.	-40.	-75.	-150.
N22	S	18.88	-108.93	24SEP84	30	-23.8	-43.0	26.9	4.0	20.	-30.	-45.	-150.
N23	S	18.90	-108.83	24SEP84	31	-14.0	-48.8	26.9	4.5	10.	-30.	-45.	-150.
N24	S	18.91	-108.93	24SEP84	31	-21.8	-40.8	26.9	5.0	10.	-35.	-50.	-150.
N26	F	18.93	-109.68	24SEP84	101	-83.6	7.0	27.6	3.0	5.	-30.	-50.	-200.
N31	F	19.81	-109.40	24SEP84	123	-0.1	52.3	27.4	5.5	5.	-30.	-50.	-200.
J 2	F	28.61	-73.77	11OCT84	1306	-130.5	-147.7	25.1	2.0	40.	-65.	-75.	-200.
J 3	F	28.83	-73.48	11OCT84	1300	-103.1	-119.8	26.0	3.0	25.	-80.	-90.	-200.
J 4	F	29.03	-73.20	11OCT84	1255	-76.3	-94.2	24.8	2.0	65.	-45.	-55.	-200.
J 7	F	29.37	-72.28	11OCT84	936	0.0	0.0	25.7	2.0	-5.	-75.	-90.	-200.
J 8	S	29.07	-72.22	11OCT84	931	11.1	-26.3	26.0	2.0	0.	-45.	-60.	-200.
J13	F	29.28	-70.52	11OCT84	1004	196.7	19.2	24.7	2.5	75.	-40.	-55.	-200.
J14	S	29.30	-70.70	11OCT84	1001	176.4	18.3	24.5	3.0	75.	-50.	-65.	-200.
J17	S	29.33	-71.97	11OCT84	943	35.3	0.6	25.8	2.0	-15.	-70.	-90.	-200.
J20	S	30.40	-71.38	11OCT84	1041	87.2	101.2	24.4	2.5	55.	-55.	-70.	-200.
J21	F	30.66	-71.20	11OCT84	1054	103.8	126.6	24.7	3.0	65.	-43.	-53.	-200.
J25	F	27.93	-71.76	11OCT84	912	78.9	-122.0	25.9	1.5	0.	-60.	-67.	-200.
J26	F	27.75	-71.65	11OCT84	909	93.7	-136.4	26.2	1.5	-5.	-65.	-75.	-200.
J27	F	27.57	-71.55	11OCT84	903	107.1	-150.3	26.0	2.5	5.	-70.	-80.	-200.
J29	F	27.41	-72.23	11OCT84	854	34.5	-176.7	26.0	2.0	30.	-30.	-50.	-200.
G 5	S	28.31	-74.09	26SEP85	950	13.7	-125.0	25.8	4.5	15.	-33.	-76.	-200.
G 7	S	28.15	-73.90	26SEP85	946	26.8	-147.6	25.8	4.0	0.	-40.	-75.	-200.
G11	S	29.86	-74.22	26SEP85	833	95.2	34.6	24.7	2.0	55.	-51.	-58.	-200.
G12	S	29.40	-74.78	26SEP85	842	16.4	20.8	26.1	5.0	45.	-33.	-69.	-200.
G13	S	28.46	-75.87	26SEP85	903	-140.1	-10.9	26.0	4.5	45.	-44.	-78.	-200.
G15	S	28.13	-76.26	26SEP85	910	-195.7	-21.6	26.4	2.5	-25.	-36.	-65.	-200.
G16	S	30.23	-73.83	26SEP85	825	152.8	49.0	25.7	2.0	-45.	-50.	-69.	-200.
G17	F	30.43	-73.61	26SEP85	821	184.8	56.2	25.5	1.5	-35.	-55.	-73.	-200.
G18	F	29.95	-74.89	26SEP85	604	82.7	112.1	25.6	1.5	-15.	-40.	-55.	-200.
G19	F	29.79	-74.89	26SEP85	620	70.3	94.4	27.2	3.0	a	-75.	-113.	a
G21	S	29.47	-74.91	26SEP85	558	61.5	72.9	26.5	3.5	-80.	-53.	-80.	-200.
G24	S	28.93	-74.92	26SEP85	550	39.3	28.4	26.5	4.5	30.	-45.	-65.	-200.
G25	F	28.91	-73.16	26SEP85	729	179.5	-85.9	26.5	3.5	-50.	-58.	-84.	-200.
G27	S	28.87	-73.85	26SEP85	720	112.5	-52.4	26.7	4.0	-40.	-55.	-95.	-200.
G31	F	28.68	-77.00	26SEP85	637	-193.4	100.4	27.7	3.0	-80.	-57.	-66.	-200.

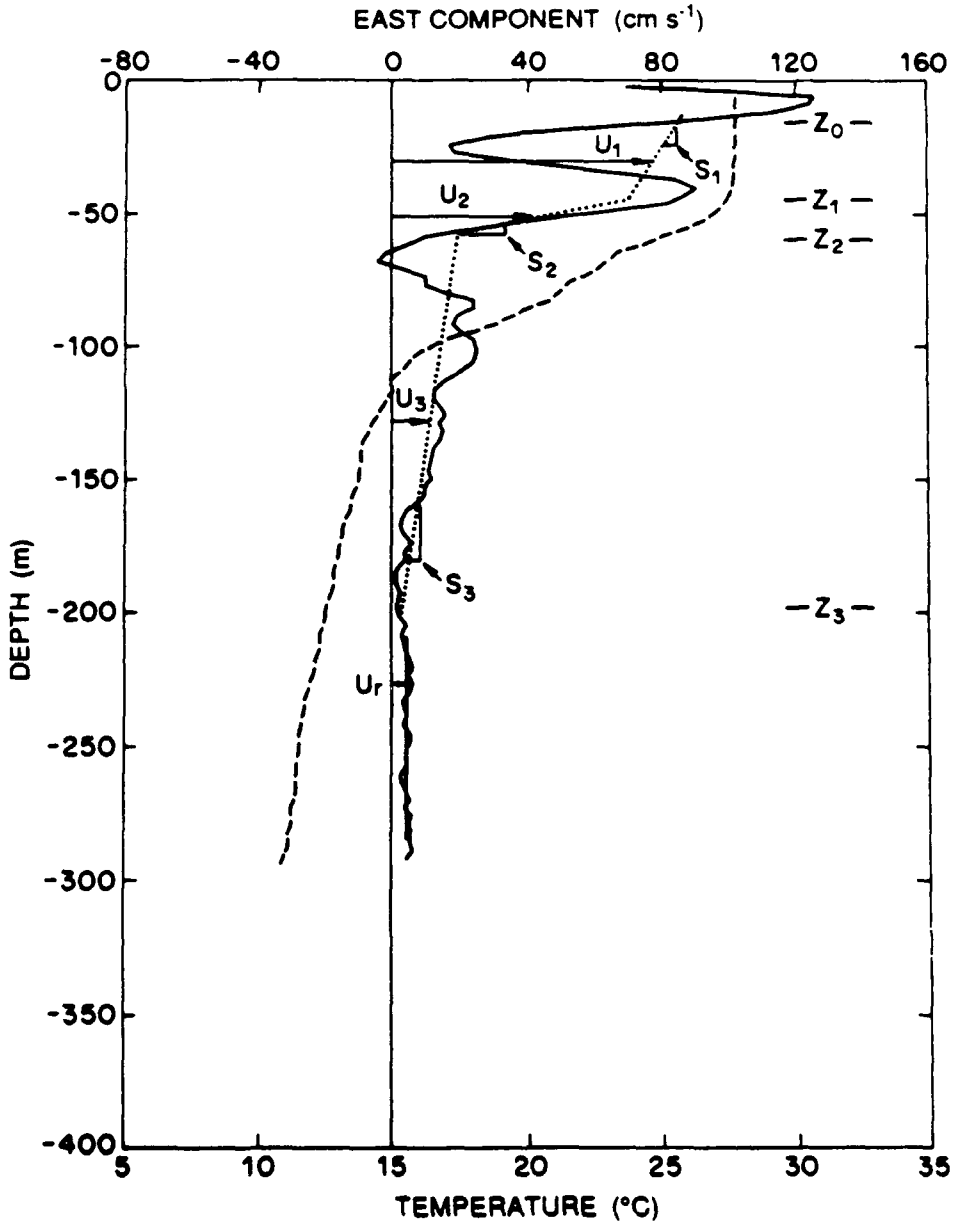

Figure 2A. Three-layer model fit to an AXCP current and temperature profile.

For most of our purposes it was necessary to separate the currents from the wave orbital motions, and it was convenient to work with layer-averaged current and shear rather than an arbitrary profile. We have therefore fitted the observed profiles to a model comprised of a single surface wave and a three-layer linear current profile, $L(z)$. For the east component,

$$U(z) = e^{kz}\left[a\cos(\omega z/W) + b\sin(\omega z/W)\right] + L(z) \quad ,$$

where $k = \omega^2/g$ is the vertical wavenumber, ω is the wave frequency estimated from the observed wave oscillation and given the known fall rate, W, and g is the acceleration due to gravity. The coefficients a, b are found by the fitting, and note that the surface amplitude of the wave is just $U_W = (a^2 + b^2)^{1/2}$. $L(z)$ is the current profile

$$\begin{aligned} &= U_1 + U_{Z1}\left(Z - \frac{Z_1}{2}\right) && \text{if } Z_0 > z \geq Z_1 \\ L(z) &= U_2 + U_{Z2}\left(Z - \frac{Z_1 + Z_2}{2}\right) && \text{if } Z_1 > z \geq Z_2 \\ &= U_3 + U_{Z3}\left(Z - \frac{Z_2 + Z_3}{2}\right) && \text{if } Z_2 > z \geq Z_3 \end{aligned}$$

where Z_0 is the start of usable data, Z_1, Z_2, Z_3 are the depths of the layers, and U_i and U_{Zi} are the depth-averaged current and shear found in layer i by the fitting procedure. They are constrained to yield a continuous profile, i.e. at the base of layer 1,

$$U_1 + \frac{U_{Z1}\,Z_1}{2} = U_2 + U_{Z2}\,\frac{Z_1 - Z_2}{2} \quad .$$

The layer depths Z_i were chosen subjectively based upon the observed structure of the temperature and current profiles, and with a definite physical

model in mind. Layer 1 is the surface mixed layer (SML) over which temperature is uniform though current may not be; layer 2 is the transition layer at the base of the SML which is strongly sheared and stratified; layer 3 is the upper thermocline. This three-layer model seemed apt for most of the profiles, and especially those with strong hurricane-driven currents. This can be judged in part by noting that the root mean square current which could not be accounted by the fit, R, was typically about 8 cm s^{-1} (see Tables 1 and 2 of Part 1, and Table 2A here).

The only troublesome aspect of the fitting procedure arose in cases where we had a fast-fall AXCP and a shallow SML (most common in Norbert). In that circumstance the shear within the SML and the wave velocity may be almost indistinguishable. Because they are not orthogonal, the fitting procedure has a tendency to return compensating estimates for shear and wave coefficients which are likely to be too large. To investigate this, we carried out a series of sensitivity tests using synthetic current profiles (reported in Part 1). We found that the coefficient of variation for shear estimates is large, about 1, but that the estimates were unbiased. We expect a simlar result to obtain in the present analysis; individual shear estimates may have O(1) uncertainty, but we expect that an average over many samples will be unbiased.

c) Storm-Centered Coordinate System

The AXCPs were dropped over a period of about four hours during which the hurricanes moved a significant distance. In order to produce a quasi-synoptic field we have therefore plotted AXCP data in a storm-centered coordinate system

Table 2A: Coefficients for three-layer model fit to Gloria AXCP profiles.

D # is the AXCP number. Z_0 is the start of usable data (m). TML is the temperature of the surface mixed layer (C) P is the period of the surface wave (s), and a and b are the cosine and sine coefficients of the fit to the surface wave (cm s^{-1}). The first row of data for each AXCP is the east component and the second row is the north component (all directions are true). Z_i is the depth of the bottom of layer i (m), U_i is the mean current in the layer (cm s^{-1}), and U_{zi} is the shear (cm s^{-1} m^{-1}). The reference velocity has been subtracted away. R is the rms difference between the observed and the best fit profile (cm s^{-1}). The format of this table exactly follows Tables 1 and 2 of Part 1 which give Norbert and Josephine data.

D #	Z_0/TML		P	a	b	Z_1	U_1	U_{Z1}	Z_2	U_2	U_{Z2}	Z_3	U_3	U_{Z3}	R
G 5	0	U	11	65	-28	-33	105	0.40	-76	43	2.58	-200	-6	-0.11	4
	25.8	V	10	30	55	-33	88	1.15	-76	42	1.23	-200	15	0.01	5
G 7	0	U	10	52	41	-40	118	0.96	-75	41	3.26	-200	-16	0.01	3
	25.8	V	10	57	-94	-40	71	0.03	-75	44	1.48	-200	17	0.02	9
G11	0	U	15	0	18	-51	-40	-0.68	-58	-20	-0.80	-200	-16	-0.01	6
	24.7	V	15	41	1	-51	81	1.17	-58	25	7.90	-200	-1	-0.02	7
G12	0	U	12	59	-64	-33	-72	-0.66	-69	-29	-1.79	-200	0	0.06	8
	26.1	V	12	2	85	-33	107	0.69	-69	53	2.35	-200	9	0.03	6
G13	0	U	10	-1	40	-44	-21	0.18	-78	-13	-0.71	-200	-2	0.01	3
	26.0	V	10	-61	-14	-44	-30	-0.13	-78	-19	-0.50	-200	-4	-0.09	6
G15	0	U	13	18	-27	-36	-31	0.02	-65	-9	-1.51	-200	7	0.09	6
	26.4	V	13	-5	-24	-36	-69	0.06	-65	-50	-1.37	-200	-18	-0.17	7
G16	0	U	13	39	-19	-50	-50	-0.41	-69	-40	0.03	-200	-29	-0.17	5
	25.7	V	13	-101	64	-50	58	0.96	-69	19	1.53	-200	1	0.05	6
G17	0	U	14	-36	89	-55	-54	-0.18	-73	-51	0.23	-200	-37	-0.24	4
	25.5	V	12	73	-90	-55	24	0.13	-73	4	1.88	-200	-4	-0.15	5
G18	O	U	12	113	-95	-40	-52	0.10	-55	-41	-1.70	-200	-22	-0.08	4
	25.6	V	13	-105	22	-40	29	0.48	-55	9	1.26	-200	4	-0.05	6
G19	-10	U	13	-213	-54	-75	-92	-1.30	-113	-43	-0.36	a	a	a	6
	27.2	V	13	189	33	-75	68	-0.02	-113	43	1.28	a	a	a	11
G21	0	U	12	-61	-34	-53	-57	0.26	-80	-35	-2.11	-200	-3	-0.07	7
	26.5	V	12	89	5	-53	41	-0.20	-80	36	0.79	-200	22	0.06	7
G24	0	U	13	51	15	-45	-84	-1.14	-65	-24	-3.47	-200	7	0.07	6
	26.5	V	12	46	-1	-45	39	-0.20	-65	25	1.83	-200	0	0.10	8
G25	0	U	9	-13	45	-58	97	-0.07	-84	65	2.58	-200	26	0.10	2
	26.5	V	9	136	-37	-58	132	1.56	-84	49	2.87	-200	5	0.13	3
G27	0	U	10	45	70	-55	40	0.51	-95	23	0.12	-200	17	0.08	4
	26.7	V	9	99	-8	-55	166	1.19	-95	79	2.72	-200	16	0.17	6
G31	0	U	11	46	-51	-57	-19	-1.17	-66	11	0.83	-200	5	0.03	3
	27.7	V	11	0	9	-57	1	-0.21	-66	4	0.74	-200	3	0.04	2

whose origin is the hurricane eye position X_c at the center time of the survey, t_c (Table II). Thus a drop made at time $t_d = t_c + \Delta t$ and at position $X_d = X_c + \Delta X$ would have a storm-centered coordinate

$$X = X_d - X_c + \Delta t \, U_H \quad ,$$

where U_H is the hurricane translation speed (assumed constant during the duration of the flight).

Finally, to simplify comparison of the three cases, the coordinate X is rotated into a frame in which U_H is up the page. The coordinates are then termed along-track and across-track, and listed in Table 1A as $(X,\ Y)$; the corresponding current and shear components are in Table 3A.

Table 3A: AXCP current data in the storm-centered coordinate system.

D # is the AXCP number; N denotes Norbert, J, Josephine, G, Gloria. U_W and V_W are the along- and across-track amplitude of the wave component at the surface (direction is ambiguous to 180°). U_i and V_i are the along- and across-track currents averaged over layer i, and U_{zi}, V_{zi} are the corresponding shears.
a: AXCP G19 did not go deep enough to measure layer 3.

D #	U_W	V_W	U_1	V_1	U_{Z1}	V_{Z1}	U_2	V_2	U_{Z2}	U_{Z2}	U_3	V_3	U_{Z3}	V_{Z3}
	(cm s^{-1})		(cm s^{-1})		(cm s^{-1} m^{-1})		(cm s^{-1})		(cm s^{-1} m^{-1})		(cm s^{-1})		(cm s^{-1} m^{-1})	
N 2	63.	18.	17.	16.	0.21	-0.03	11.	3.	0.03	1.06	2.	-6.	0.14	-0.07
N 3	-84.	33.	-43.	-101.	-0.50	-0.48	-23.	-55.	-1.36	-4.30	-10.	-6.	-0.03	-0.14
N 4	-91.	-132.	11.	21.	-0.19	-1.56	6.	21.	0.43	1.34	-1.	-7.	-0.01	0.07
N 6	110.	221.	29.	73.	-0.53	1.41	23.	29.	1.83	3.02	4.	2.	0.08	0.06
N13	-80.	17.	80.	51.	-0.41	0.74	35.	8.	2.97	1.72	-18.	-15.	0.01	-0.12
N14	-10.	104.	80.	-3.	1.03	0.36	27.	-13.	3.12	0.34	-11.	-16.	-0.02	-0.01
N15	-23.	17.	-68.	73.	-0.50	0.65	-31.	33.	-2.40	2.53	0.	1.	-0.02	-0.01
N16	20.	42.	-10.	87.	1.09	0.69	-15.	30.	-1.15	3.55	1.	-6.	-0.02	-0.12
N18	-41.	134.	54.	-29.	3.31	-0.43	21.	-27.	-0.48	0.26	11.	-26.	0.51	-0.11
N20	30.	111.	21.	-105.	-0.09	-2.93	16.	-53.	0.46	-1.18	-3.	-18.	0.19	-0.30
N21	-126.	-43.	-18.	-99.	-0.19	-0.54	-4.	-65.	-0.57	-1.43	-2.	-23.	0.19	-0.47
N22	-34.	54.	59.	-26.	1.19	-0.15	25.	-21.	2.06	-0.41	3.	-5.	0.13	-0.25
N23	17.	90.	77.	-33.	3.19	-1.41	18.	-17.	1.45	0.71	1.	-6.	0.13	-0.32
N24	-7.	81.	43.	-33.	1.37	0.39	5.	-39.	1.87	-0.23	-16.	-21.	0.14	-0.30
N26	-190.	86.	-13.	0.	-1.98	-0.20	11.	7.	-0.18	-0.41	3.	4.	0.14	0.09
N31	63.	53.	-65.	21.	-5.08	-0.29	15.	16.	-0.31	0.93	8.	-1.	0.12	0.10
J 2	-9.	-69.	11.	15.	0.07	0.02	9.	9.	0.08	0.94	4.	1.	0.07	0.05
J 3	1.	59.	6.	43.	-0.03	-0.14	15.	38.	-1.52	2.08	16.	20.	0.13	0.15
J 4	76	-28.	-3.	24.	0.75	-0.63	-16.	18.	-0.76	4.22	-11.	1.	-0.03	-0.05
J 7	-73.	22.	9.	43.	-0.18	0.45	11.	2.	0.76	3.18	5.	-14.	0.00	-0.13
J 8	38.	-3.	30.	16.	0.26	0.10	5.	5.	2.69	1.30	-7.	-3.	-0.11	-0.02
J13	-122.	10.	36.	21.	-1.75	-0.27	43.	17.	3.76	1.19	14.	7.	0.01	0.03
J14	14.	-43.	33.	29.	0.07	0.49	16.	8.	2.12	1.06	2.	0.	-0.03	0.01
J17	-22.	-40.	44.	58.	0.06	0.46	30.	11.	1.28	3.05	14.	-15.	0.05	-0.09
J20	-25.	20.	-8.	25.	-0.07	0.28	-13.	7.	0.91	1.25	-16.	0.	-0.06	-0.03
J21	18.	50.	-3.	15.	0.34	-0.78	-8.	10.	-0.33	4.31	-5.	-7.	-0.02	-0.06
J25	12.	73.	20.	12.	0.35	0.25	6.	16.	1.03	-3.21	-2.	19.	0.07	0.12
J26	24.	50.	4.	-2.	-0.01	0.15	-4.	-1.	1.55	-0.96	-9.	-1.	-0.04	0.06
J27	137.	-29.	-1.	15.	0.18	0.01	-11.	11.	0.84	0.61	-13.	5.	-0.03	0.04
J29	-18.	-13.	-1.	-14.	1.11	1.86	-15.	-12.	-0.16	-2.99	-10.	20.	-0.05	-0.04
G 5	90.	39.	133.	31.	0.88	0.84	57.	18.	2.86	-0.08	1.	16.	-0.09	0.06
G 7	99.	85.	138.	10.	0.88	-0.41	57.	21.	3.57	-0.16	-6.	22.	0.02	0.02
G11	30.	31.	2.	90.	-0.08	1.35	-6.	31.	2.87	7.40	-15.	6.	-0.02	-0.02
G12	106.	61.	-15.	128.	-0.28	0.92	-2.	60.	-0.52	2.91	4.	8.	0.06	0.00
G13	-59.	-53.	-32.	-17.	0.10	-0.19	-21.	-11.	-0.86	-0.13	-4.	-3.	-0.03	-0.09
G15	27.	-29.	-59.	-47.	0.05	0.05	-31.	-40.	-1.97	-0.54	-2.	-19.	0.01	-0.19
G16	-14.	-123.	-18.	74.	0.07	1.04	-27.	35.	0.72	1.35	-26.	14.	-0.13	0.12
G17	-37.	139.	-37.	46.	-0.10	0.19	-44.	27.	1.06	1.57	-35.	13.	-0.28	-0.02
G18	96.	-138.	-33.	49.	0.31	0.38	-32.	27.	-0.95	1.89	-18.	13.	-0.10	-0.01
G19	-117.	254.	-51.	102.	-1.17	0.57	-19.	58.	0.26	1.31	0.	0.	0.00	0.00
G21	-24.	109.	-32.	63.	0.14	-0.29	-15.	49.	-1.52	1.67	a	a	a	a
G24	71.	22.	-57.	73.	-1.11	0.34	-10.	33.	-2.26	3.20	6.	-3.	0.10	0.06
G25	84.	142.	146.	74.	0.65	1.42	80.	15.	3.60	1.38	25.	-8.	0.15	0.06
G27	114.	58.	111.	130.	0.99	0.83	57.	60.	1.35	2.37	22.	6.	0.15	0.12
G31	70.	-6.	-17.	10.	-1.14	0.35	11.	-2.	1.08	0.28	5.	0.	0.01	-0.04

DOCUMENT LIBRARY

March 11, 1991

Distribution List for Technical Report Exchange

Attn: Stella Sanchez-Wade
Documents Section
Scripps Institution of Oceanography
Library, Mail Code C-075C
La Jolla, CA 92093

Hancock Library of Biology &
Oceanography
Alan Hancock Laboratory
University of Southern California
University Park
Los Angeles, CA 90089-0371

Gifts & Exchanges
Library
Bedford Institute of Oceanography
P.O. Box 1006
Dartmouth, NS, B2Y 4A2, CANADA

Office of the International
Ice Patrol
c/o Coast Guard R & D Center
Avery Point
Groton, CT 06340

NOAA/EDIS Miami Library Center
4301 Rickenbacker Causeway
Miami, FL 33149

Library
Skidaway Institute of Oceanography
P.O. Box 13687
Savannah, GA 31416

Institute of Geophysics
University of Hawaii
Library Room 252
2525 Correa Road
Honolulu, HI 96822

Marine Resources Information Center
Building E38-320
MIT
Cambridge, MA 02139

Library
Lamont-Doherty Geological
Observatory
Colombia University
Palisades, NY 10964

Library
Serials Department
Oregon State University
Corvallis, OR 97331-5503

Pell Marine Science Library
University of Rhode Island
Narragansett Bay Campus
Narragansett, RI 02882

Working Collection
Texas A&M University
Dept. of Oceanography
College Station, TX 77843

Library
Virginia Institute of Marine Science
Gloucester Point, VA 23062

Fisheries-Oceanography Library
151 Oceanography Teaching Bldg.
University of Washington
Seattle, WA 98195

Library
R.S.M.A.S.
University of Miami
4600 Rickenbacker Causeway
Miami, FL 33149

Maury Oceanographic Library
Naval Oceanographic Office
Stennis Space Center
NSTL, MS 39522-5001

Marine Sciences Collection
Mayaguez Campus Library
University of Puerto Rico
Mayagues, Puerto Rico 00708

Library
Institute of Oceanographic Sciences
Deacon Laboratory
Wormley, Godalming
Surrey GU8 5UB
UNITED KINGDOM

The Librarian
CSIRO Marine Laboratories
G.P.O. Box 1538
Hobart, Tasmania
AUSTRALIA 7001

Library
Proudman Oceanographic Laboratory
Bidston Observatory
Birkenhead
Merseyside L43 7 RA
UNITED KINGDOM

50272-101

REPORT DOCUMENTATION PAGE	1. REPORT NO. WHOI-91-06	2.	3. Recipient's Accession No.

4. Title and Subtitle

Ocean Response to a Hurricane, Part II:
Data Tabulations and Numerical Modeling

5. Report Date January, 1991

6.

7. Author(s)

James F. Price, Thomas B. Sanford and George Z. Forristall

8. Performing Organization Rept. No. WHOI 91-06

9. Performing Organization Name and Address

The Woods Hole Oceanographic Institution
Woods Hole, Massachusetts 02543

10. Project/Task/Work Unit No.

11. Contract(C) or Grant(G) No.

(C)

(G) N00014-89-J-1053

12. Sponsoring Organization Name and Address

Funding was provided by the Office of Naval Research

13. Type of Report & Period Covered

Technical Report

14.

15. Supplementary Notes

This report should be cited as: Woods Hole Oceanog. Inst. Tech. Rept., WHOI-91-06.

16. Abstract (Limit: 200 words)

Field observations of the ocean's forced stage response to three hurricanes, Norbert (1984), Josephine (1984) and Gloria (1985), are analyzed and presented in a storm-centered coordinate system. All three hurricanes had a non-dimensional speed of O(1) and produced a strongly rightward biased response of the ocean surface mized layer (SML) transport and current. The maximum layer-averaged SML currents varied from 0.8 m s^{-1} in response to Josephine, which was a fairly weak hurricane, to 1.7 m s^{-1} in response to Gloria, which was much stronger. In these two cases the current amplitude is set primarily by the strength of the wind stress and its efficiency of coupling with the SML current, and the depth of vertical mixing of the SML. The Norbert case (SML Burger number $\simeq 1/2$) was also affected by significant pressure-coupling with the thermocline that caused appreciable upwelling by inertial pumping and strong thermocline-depth currents, up to 0.3 m s^{-1}, under the trailing edge of Norbert. The observed SML current has a vertical shear in the direction of the local wind of up to 0.01 s^{-1}. This vertical shear causes the surface current to be larger than the layer-averaged SML current described above by typically 0.2 m s^{-1}.

17. Document Analysis a. Descriptors

1. ocean models
2. wind-driven currents
3. aircraft measurements

b. Identifiers/Open-Ended Terms

c. COSATI Field/Group

18. Availability Statement	19. Security Class (This Report)	21. No. of Pages
Approved for publication; distribution unlimited.	UNCLASSIFIED	71
	20. Security Class (This Page)	22. Price

(See ANSI-Z39.18) *See Instructions on Reverse* OPTIONAL FORM 272 (4-77) (Formerly NTIS-35) Department of Commerce